Supplement of Atmos. Chem. Phys., 18, 10055–10088, 2018
https://doi.org/10.5194/acp-18-10055-2018-supplement

Atmospheric Chemistry and Physics
Open Access
EGU

Supplement of

Long-term study on coarse mode aerosols in the Amazon rain forest with the frequent intrusion of Saharan dust plumes

Daniel Moran-Zuloaga et al.

Correspondence to: Daniel Moran-Zuloaga (daniel.moran@mpic.de) and Christopher Pöhlker (c.pohlker@mpic.de)

S1 Supplementary information relating to materials and methods

S1.1 Inlet aspiration and transmission efficiency with particle loss corrections

According to von der Weiden et al. (2009), the following aspects have to be considered in terms of particle loss mechanisms:

(i) *Isoaxial sampling*: The TSP inlet head at the ATTO site aspires air from all directions.

(ii) *Isokinetic sampling*: At the ATTO site, the wind speed at the TSP inlet head typically varies in the range 2.0 ± 0.5 m s^{-1} (mean ± one standard deviation). Accordingly, the sampling took place in moving air, which probably caused unavoidable biases due to non-isokinetic sampling.

(iii) *Sedimentation*: Sedimentation losses occur in inclined tube sections for particles >0.5 µm. The horizontal distance between the inlet head and instruments has been reduced as far as possible (i.e., the instrument container is located right at the foot of the mast) to minimize the length of inclined sections and, thus, sedimentation losses in the tubes. However, the remaining effect of the sedimentation (i.e., of large particles) is the dominant loss mechanisms in this context. The subsequently presented loss correction functions take this effect into account.

(iv) *Diffusion*: Diffusive losses due to Brownian motion of particles and their adsorption at the tube's walls is relevant for particle sizes <100 nm and can be neglected here.

(v) *Turbulent inertial deposition*: The flow rates in the inlet have been optimized to minimize the residence time of the air in the tubes (~90 sec) as far as the *laminar flow regime* allows (Reynolds number Re < 2000) (Seinfeld and Pandis, 2006; Baron et al., 2011).

(vi) *Inertial deposition in bends, contractions, and/or enlargements*: Sharp bends in the tubes have been avoided. The numbers of contractions and enlargements in the tube diameter have been minimized. The unavoidable inertial deposition effects in this context are covered by the loss correction functions.

(vii) *Electrostatic deposition*: The entire inlet system is grounded and consists of electrically conducting materials (i.e., stainless steel and conducting rubber tubes) to avoid electrostatic deposition.

(viii) The effects of thermophoresis, diffusiophoresis, interception, and coagulation can be neglected in the context of the present study.

Although the inlet design has been optimized to achieve a maximum sampling efficiency, a certain extent of particle losses is unavoidable. Thus, we calculated the effective aerosol transmission (i.e., for the OPS size range) in the inlet by using the particle loss calculator (PLC, version 2.0) software package that has been developed by von der Weiden et al. (2009). For these calculations, we implemented the design of the aerosol inlet at the ATTO site into the PLC. Note that the inlet configuration (i.e., the design of aerosol dryer) has been modified twice, in May 2014 and January 2015. Inlet modification became necessary due to the growing number of online instruments at the aerosol inlet. Specifically, the drying system was upgraded, which impacted the overall geometry of the split and distribution of sample air to the individual instruments inside the laboratory container. Accordingly, three different inlet designs have been used throughout this study (see

Fig. 1). The PLC calculations were conducted for all three designs to account for the respective design differences. Furthermore, aerosol losses were calculated with a constant temperature of 30°C and a pressure of 1013 hPa, in order to reflect the conditions in the air-conditioned container.

Besides the inlet design, the properties of the actual aerosol particles (i.e., their shape and density) have a significant influence on their aerodynamic properties, inertial effects, gravitational settling, and, thus, the inlet transmission function. However, the particle's shape and density are typically unknown for the complex ambient aerosol population. Thus, a standard density of 1 g cm^{-3} ($\rho_{1.0}$) and a standard shape factor of 1 (corresponding to spherical particles) were applied here. For the coarse mode aerosol at the ATTO site it is known that PBAP, mineral dust, and sea salt represent the dominant constituents (see Sect. S2.2). Accordingly, we conducted a sensitivity test regarding the density influence on the PLC results. Table S1 summarizes measured densities as reported in the literature. Based on these values, we selected the following densities as test cases: (i) A lower limit density of 0.85 g cm^{-3} ($\rho_{0.85}$) was chosen and corresponds to typical pollen densities and therefore represents 'light' PBAP particles. (ii) The standard density of 1 g cm^{-3} ($\rho_{1.0}$) was chosen as 'best guess' for typical PBAP densities. (iii) A density of 1.2 g cm^{-3} ($\rho_{1.2}$) represents (an upper limit of) typical fungal spore densities. (iv) A large density of 2.0 g cm^{-3} ($\rho_{2.0}$) as a representative density for pure mineral dust and sea salt particles.

Figure S1 show that the aerosol transmission function starts at about 1 (full transmission) for particles around 0.7 µm and then declines with increasing particle size. It can be seen that the choice of the particle density (i.e., $\rho_{0.85}$, $\rho_{1.0}$, $\rho_{1.2}$, and $\rho_{2.0}$) for the PLC has a much larger effect on the resulting transmission functions than the three different inlet designs at the ATTO site that we implement into the calculation. While the specific designs of the inlet systems can be implemented into the PLC rather precisely, the assumed average density introduces an inherent uncertainty into the calculation. Throughout the study, $\rho_{1.0}$ was chosen as the *default* representation of the average properties of the coarse mode particles at the ATTO site (compare Table 1). We have used $\rho_{1.0}$ in both, the PLC correction as well as in the conversion of number size distributions to mass size distributions. However, we are aware of the fact that this choice may underestimate the total aerosol mass concentration (M) during episodes when mineral dust advection prevails (i.e., when densities approach $\rho_{2.0}$) and potentially overestimates M during episodes with prevalence of 'light' bioaerosols (e.g., pollen with densities close to $\rho_{0.85}$). For $\rho_{1.0}$, the 50 % transmission efficiency of the aerosol inlet is nominally >10 µm.

S2 Supplementary text

S2.1 Aitken and accumulation mode properties in the Amazon

The Aitken mode is centered at ~0.07 µm diameter and its number concentrations, N_{Ait}, ranges from ~100 to ~500 cm^{-3} (Martin et al., 2010; Andreae et al., 2015; M. Pöhlker et al., 2016). Aitken mode particles in the Amazon are thought to originate at least in part from aerosol nucleation in the upper troposphere (Andreae et al., 2017), being subsequently transported into the boundary layer by vertical downdrafts as described in Krejci et al. (2003) and Wang et al. (2016). Particles at this size predominantly consist of organic constituents (Sun and Ariya, 2006; Chen et al., 2009; M. Pöhlker et al., 2016). A characteristic feature in the Amazonian atmosphere is the lack of particles smaller than Aitken mode size (i.e., <0.04 µm). This is in stark contrast to most other continental sites (i.e., with varying extents of fossil fuel combustion influence), which typically show a pronounced nucleation mode (e.g. < 0.02 µm) (Dusek et al., 2006; Kalafut-Pettibone et al., 2011).

The accumulation mode is typically the dominant mode in terms of number concentrations. Its maximum is located at ~0.150 µm, and the concentration, N_{acc}, ranges from ~100 to ~1500 cm^{-3} (Andreae et al., 2015; Pöhlker et al., 2016). Accumulation mode aerosol originates from aging of Aitken mode particles (i.e., condensational growth and/or cloud processing) (Zhou et al., 2002; Pöschl et al., 2010) and combustion emissions (Remer et al., 1998). Under pristine conditions, Amazonian accumulation mode particles are predominantly organic as they contain substantial contributions of secondary organic matter (SOM) from boundary layer oxidation of volatile organic compounds (VOC) as well as minor contributions from direct biogenic emissions (C. Pöhlker et al., 2012; Yañez-Serrano et al., 2014; Chen et al., 2015). During the dry season, the accumulation mode contains a major fraction of pyrogenic particles (Janhäll et al., 2010; Brito et al., 2014). Note that about one third of the aerosol is inorganic (ionic species) with a higher fraction of inorganics in the wet season (Artaxo et al., 1993; Rissler et al., 2006; Andreae et al., 2012). Two recent studies by M. Pöhlker (2016; 2017) showed that the accumulation mode includes the majority of cloud condensation nuclei (CCN) at typical water vapor supersaturations.

In contrast to the Aitken and accumulation modes, coarse mode particles occur in significantly lower number concentrations. The coarse mode concentration, N_c, mostly varies around ~0.5 cm^{-3} (Huffman et al., 2012; Whitehead et al., 2016). While the coarse mode contributes just a small fraction to the overall aerosol number concentration (less than 0.1 %), it constitutes a substantial, sometimes dominant, fraction of the total aerosol mass concentration, which may reach up to 70 % (Martin et al., 2010).

S2.2 Major sources of Amazonian coarse mode particles

S2.2.1 Primary biological aerosol particles

Primary biological aerosol particles (PBAP), also called bioaerosols, represent a substantial fraction of the coarse mode aerosol worldwide (Després et al., 2012; Fröhlich-Nowoisky et al., 2016). Bioaerosols typically comprise a complex mixture of microorganisms (e.g., bacteria, algae), reproductive units (e.g., pollen, fungal spores, viruses), as well as various organism fragments and debris. These particles cover a wide size range

from few nanometers to ~100 µm (Pöschl and Shiraiwa, 2015). Over the last decades, bioaerosols have received a lot of attention in the atmospheric science community due to their relevance in several climate and health-related processes. For instance, several bioaerosol classes have been identified as important allergens and pathogens (Brown and Hovmøller, 2002; Yamamoto et al., 2012). Moreover, the role of bioaerosols as ice nuclei (IN) is a very actively debated topic, since it may have major implications for cloud and precipitation formation and, thus, the hydrological cycle (Möhler et al., 2007; Morris et al., 2008; Hoose et al., 2010; Sahyoun et al., 2016; Du et al., 2017).

Since bioaerosols are directly emitted from the biosphere, the enormous diversity of biological activity in the Amazon rain forest makes it a unique location to study bioaerosol related processes. For the Amazon, previous studies have reported initial results on PBAP temporal variability and size distribution (Gilbert and Reynolds, 2005; Huffman et al., 2012), their potential impact on cloud formation and development (Prenni et al., 2009), as well as their diversity (Womack et al., 2010).

S2.2.2 Advection of Saharan dust plumes

The African continent and in particular the Saharan desert with the sub-Saharan Sahel region represent the world's largest source of dust aerosols (Prospero et al., 2014). The sequence of frequent Saharan dust outbreaks, which constitute a periodic westerly flux across the Atlantic Ocean to North and South America, is a subject of various research activities and has been studied for over a century (Darwin, 1846; Ehrenberg, 1849; Prospero et al., 1981; Andreae, 1983; Prospero, 1999). Accordingly, the large amount of matter that is transported intercontinentally and widely deposited during its journey has important implications on oceanography (Baker et al., 2010), climatology (Kaufman et al., 2005; Choobari et al., 2014; Di Biagio et al., 2017), marine and terrestrial ecology (Okin et al., 2011; Makowski Giannoni et al., 2016; Rizzolo et al., 2016), as well as on public health (Goudie, 2014). There is a large body of studies on various aspects of the emission and transport characteristics of this phenomenon. In the following paragraphs, we briefly summarize the key aspects that are of relevance for our study, while further details can be found in the referenced publications.

Overall, about 1000 Tg a^{-1} of dust are emitted from the Saharan region, transported over hundreds to thousands of kilometers, and deposited into the Atlantic Ocean, onto the American continents as well as other locations (Gläser et al., 2015). A number of source regions (i.e., in Mauretania, Mali, Algeria, Chad), which contribute to varying extent to the overall dust burden, have been identified (Formenti et al., 2011; Kumar et al., 2014; Gläser et al., 2015; Wang et al., 2016). The Bodélé depression in central Chad (17° N 18° E) represents one of the most active source regions worldwide and it has been suggested that it is of particular importance for the Amazon Basin (Koren et al., 2006; Ben-Ami et al., 2010). So far, however, this has not been confirmed by isotopic investigations (Abouchami et al., 2013; Kumar et al., 2014, 2018).

The meteorological conditions in Africa that lift the dust particles – and therefore define the activity of the source regions – follow pronounced seasonal trends (e.g., Knippertz and Todd, 2012). Also the spatiotemporal patterns of the plumes during the transatlantic passage show strong seasonal variability (Engelstaedter et al., 2009). During Northern Hemispheric summer – corresponding to the first half of the Amazonian dry

season (see Sect. 2.11) – pulses of dust are transported zonally towards the Caribbean area and typically do not reach the Amazon Basin (Prospero and Lamb, 2003). These dust plumes are typically lifted to comparably high altitudes and transported in the so called Saharan air layer (SAL), which is located on top of the marine boundary layer ranging from 2 to 5 km altitude (Kanitz et al., 2014). The scenario during the Northern Hemispheric winter – corresponding to the Amazonian wet season – is quite different. During this time of the year, the dust is predominantly transported in western to southwestern directions in the trade wind layer (Garrison et al., 2014). A considerable amount of the plume's dust burden is deposited in the Amazon Basin (Gläser et al., 2015; Wang et al., 2016). These dust plumes are mostly 'smoky' as they are mixed with large amounts of biomass burning aerosols from the savanna fires in the Sahel region (Barbosa et al., 1999; Ben-Ami et al., 2009; Knippertz et al., 2011).

With respect to the Amazonian rain forest, it has been proposed that the annual advection and deposition of dust fulfills a critical fertilizing role in this ecosystem (Bristow et al., 2010). Moreover, Yu et al. (2015) have estimated that about 29 kg ha^{-1} a^{-1} of Saharan dust are deposited in the Amazon Basin, which introduces important nutrients, e.g., phosphorus to the comparably poor Amazonian soils. A new study from Rizzolo et al., (2016) recently suggested that other imported elements, such as iron, may also play an important role in the ecosystem. Previous studies have also shown that the dust pulses transported into the Amazon Basin are typically complex mixtures of dust, biomass burning, and sea spray aerosols (Formenti et al., 2001; Baars et al., 2011; Dudley et al., 2012; Makowski Giannoni et al., 2016). While an overall conceptual understanding of the intercontinental biogeochemical 'bridge' between the Sahara and the Amazon biome exists (Talbot et al., 1990; Swap et al., 1992), a variety of questions remain unanswered.

S2.2.3 Marine aerosol

During the transatlantic passage, the Saharan dust plumes are often mixed with sea spray aerosols from the marine boundary layer (Andreae et al., 1986; Talbot et al., 1990; Ben-Ami et al., 2009; Makowski Giannoni et al., 2016). This mixing mostly occurs during Northern Hemispheric winter, when the Saharan dust plumes are transported at comparatively low altitudes (Liu et al., 2008; Knippertz et al., 2011; Wang et al., 2016). During Northern Hemispheric summer, the SAL tends to be more decoupled from the marine boundary layer, which mostly prevents mixing of dust and sea spray (Talbot et al., 1990; Fuchs and Cermak, 2015). The LRT plumes that are injected into the Amazon Basin in NH winter comprise a noticeable contribution of marine aerosol beside the dust and biomass burning constituents of African origin (Graham et al., 2003). A number of studies support this concept as they observed typical marine aerosol constituents (i.e., Na, Cl, Mg, and sulfate) in Amazonian aerosol and rain water samples (Andreae et al., 1990a; Andreae et al., 1990b; Dudley et al., 2012; Pauliquevis et al., 2012; Makowski Giannoni et al., 2016).

S2.2.4 Coarse mode fraction of biomass burning aerosols

Biomass burning is closely linked to the emission of large amounts of accumulation mode particles (Martin et al., 2010). However, also coarse mode particles are co-emitted by fires with particles sizes reaching up to

millimeters (Radke et al., 1990; Janhäll et al., 2010). The coarse mode particle fraction, which originates from biomass burning, comprises dust, carbon aggregates, ash, and unburned parts of the biomass (Janhäll et al., 2010). Furthermore, the physicochemical properties (i.e., particle size and composition) can vary as a function of the fuel (e.g., forest vs. savanna vs. grass land fires) (Janhäll et al., 2010; Simões Amaral et al., 2016). Since biomass burning is a major source of atmospheric aerosols in the Amazon region, the coarse mode tail of the emitted pyrogenic size distribution likely impacts the coarse mode aerosol population to certain, however undefined, extent. Accordingly, this pyrogenic input is relevant for the present study and makes the coarse mode composition, which is fed by diverse biogenic, desert and marine sources, even more complex.

S3 Supplementary figures

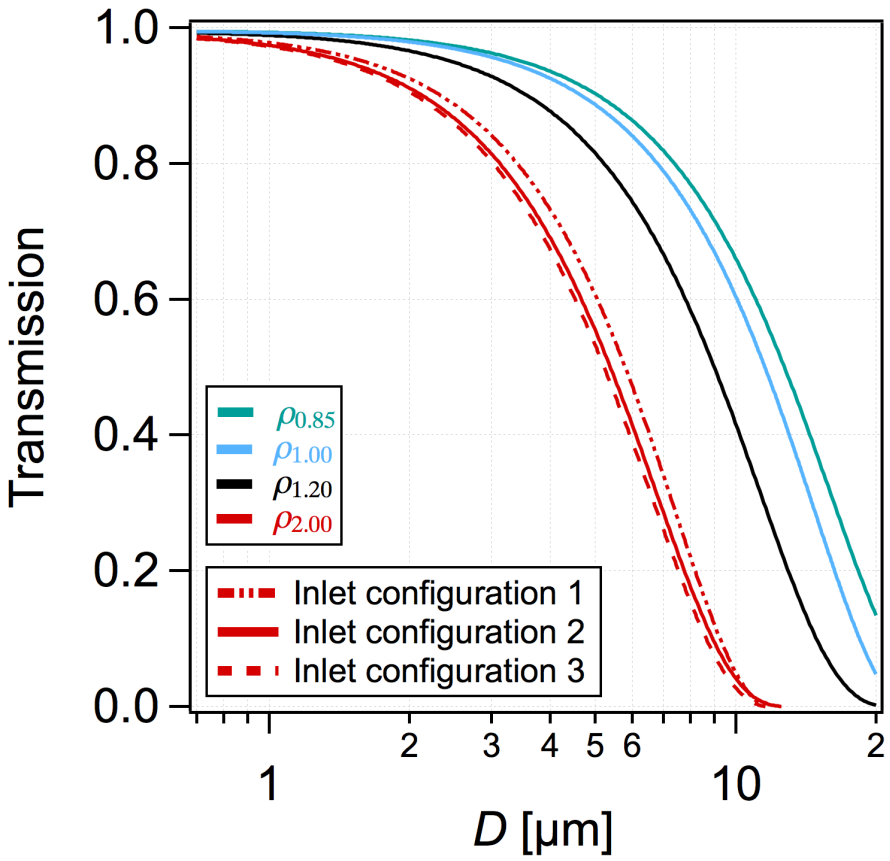

Figure S1. Calculated transmission efficiencies of the ATTO aerosol inlet (at the 80 m mast) from TSP inlet head to OPS instrument. Transmission curves were calculated for three different inlet designs (related to technical modifications at the inlet). Inlet configuration 1 corresponds to period from Jan to May 2014. Inlet configuration 2 corresponds to period May 2014 to Feb 2015. Inlet configuration 3 corresponds to period from Feb 2015 onwards. Moreover, four selected aerosol densities (i.e., $\rho_{0.85}$ representing 'light' PBAP such as pollen, $\rho_{1.0}$ representing typical PBAP density, $\rho_{1.2}$ representing upper limit for PBAP densities, and $\rho_{2.0}$, representing mineral dust and sea salt aerosol) have been implemented (see also Table S1). Transmission curves show a major influence of selected aerosol densities and minor influence of inlet design.

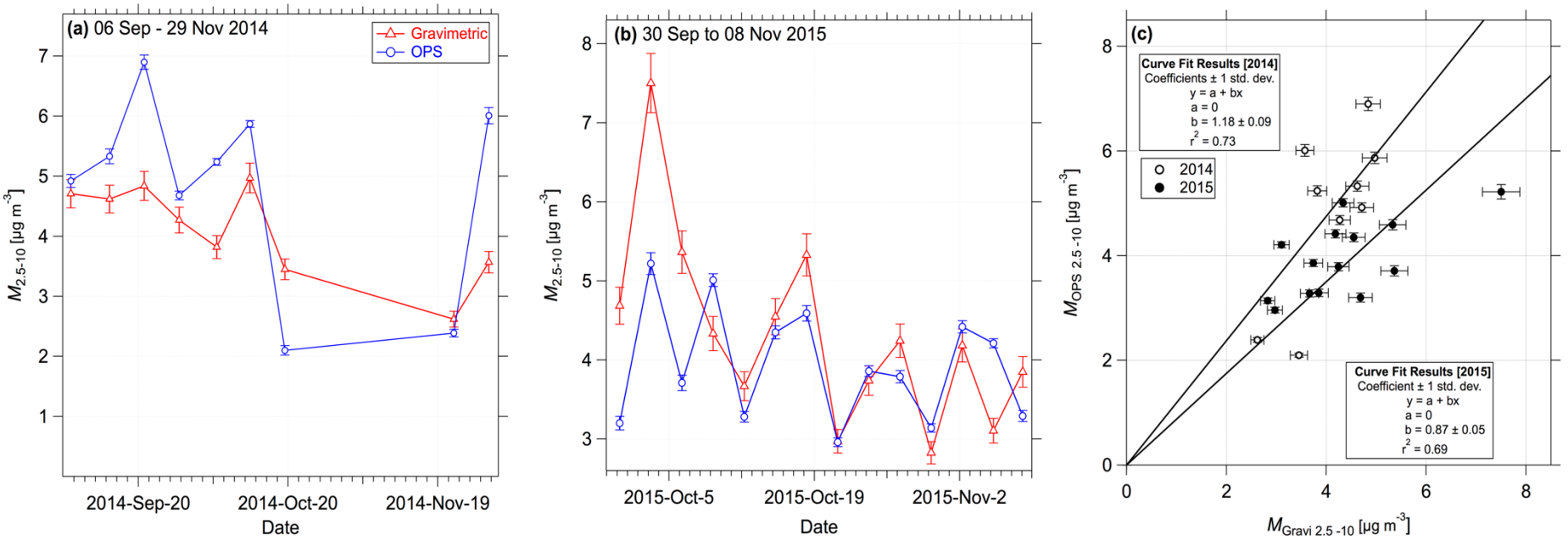

Figure S2. Comparison of OPS-based retrieval of coarse mode aerosol mass concentration vs. gravimetric analysis of aerosol filters at the ATTO site. The implemented size range of OPS data and gravimetry spans from 2.5 to 10 µm. The comparison was conducted for two periods: (**a**) 06 Sep to 29 Nov 2014 and (**b**) 30 Sep to 08 Nov 2015. Linear regression fits (forced through zero) for both periods in (**c**) confirm overall agreement of both techniques.

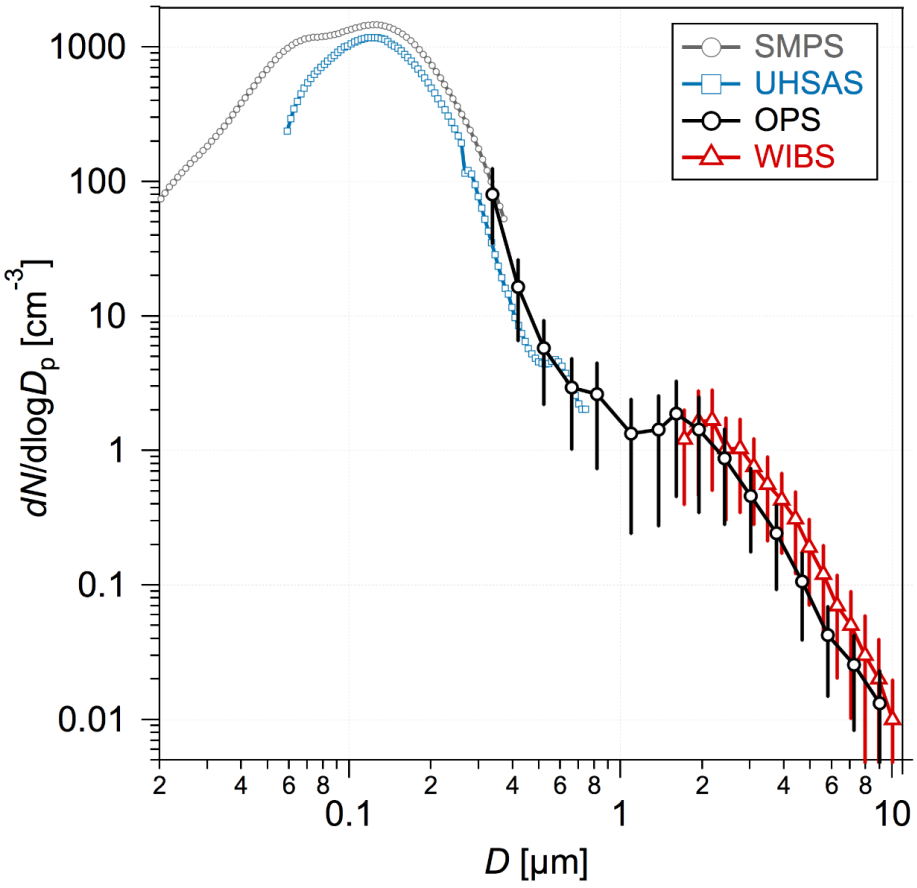

Figure S3. Intercomparison of aerosol number size distributions from a scanning mobility particle sizer (SMPS), an ultra-high sensitive aerosol spectrometer (UHSAS), an optical particle sizer (OPS), and a wideband integrated bioaerosol sensor (WIBS). Data represents the monthly average of June 2015. The lines of the distributions represent the mean values, whereas the error bars for the OPS and WIBS represents one standard deviation. The error bars for the SMPS and UHSAS data were omitted for clarity. Note that the UHSAS detection efficiency drops below ~100 nm. Overall, the individual number size distributions are in good agreement and confirm that the OPS data set is consistent with other sizing techniques that are operated at the ATTO site.

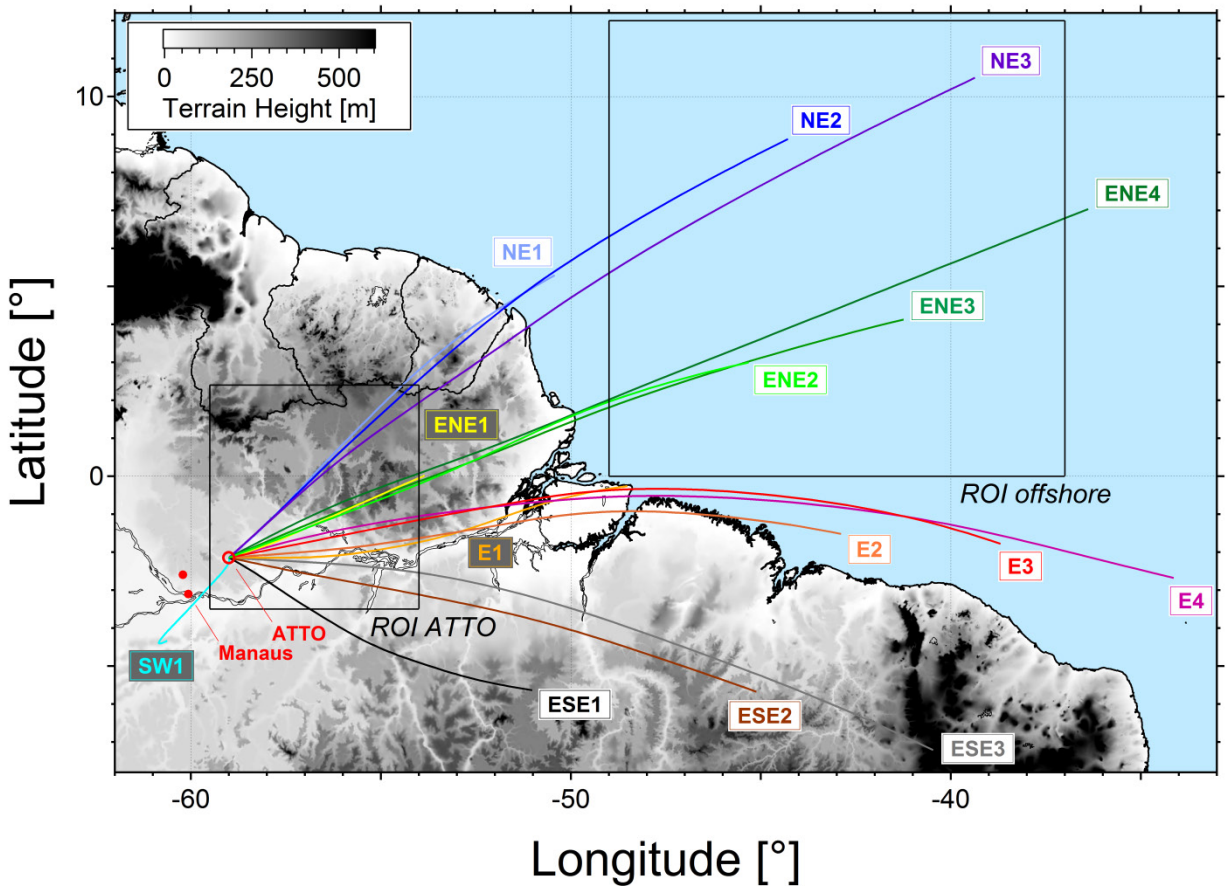

Figure S4. Map of northeast Amazon Basin with 15 final clusters from systematic back trajectory cluster analysis based on multi-year back trajectory data set – for details see (C. Pöhlker et al., 2018). Trajectory clusters show that air masses arrive at the ATTO site almost exclusively from north-eastern to south-eastern directions. Five major wind directions can be discriminated: (i) Northeasterly clusters NE1, NE2, and NE3; (ii) east-northeasterly clusters ENE1, ENE2, ENE3, and ENE4; (iii) easterly clusters E1, E2, E3, and E4; (iv) east-southeasterly clusters ESE1, ESE2, and ESE3, and (v) southwesterly cluster SW1. In the illustration are also shown the regions of interest ROI_{ATTO} and ROI_{off}. The topographic map is represented by a grey scale, which is capped at 600 m. Figure adapted from C. Pöhlker et al. (2018).

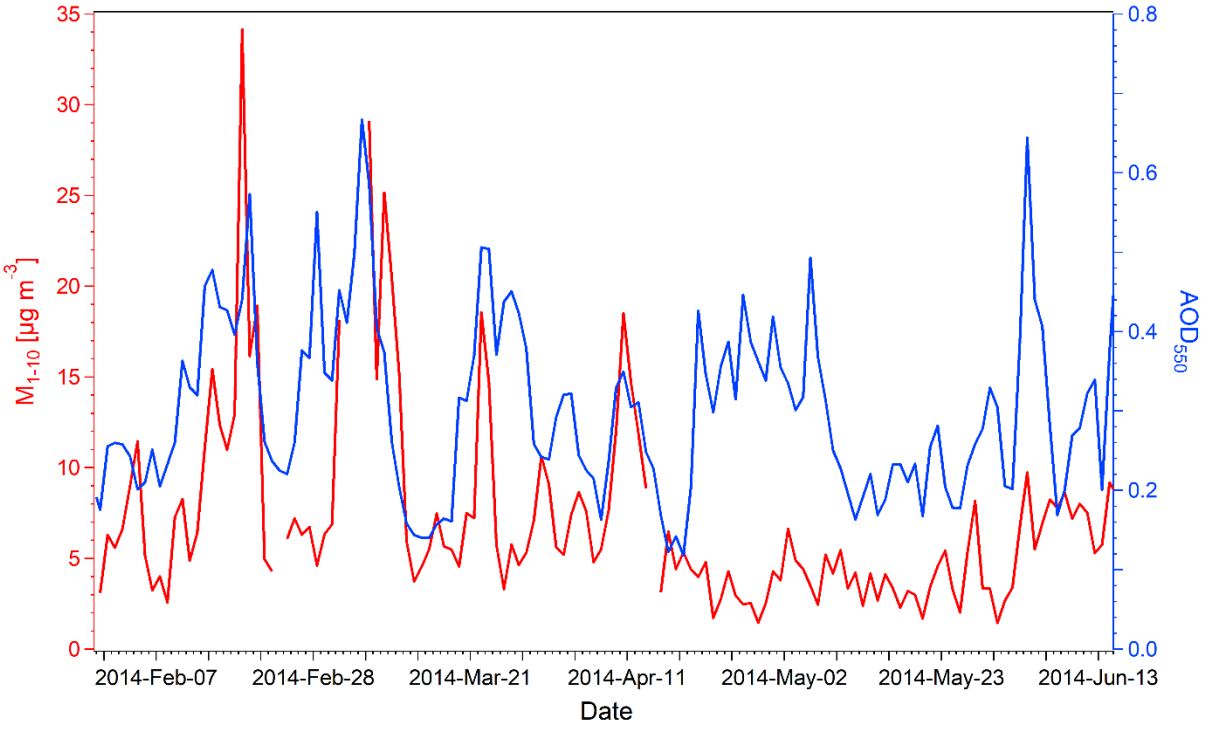

Figure S5. Comparison of $AOD_{ROI,off}$ vs. $M_{1\text{-}10}$ for the dust season 2014.

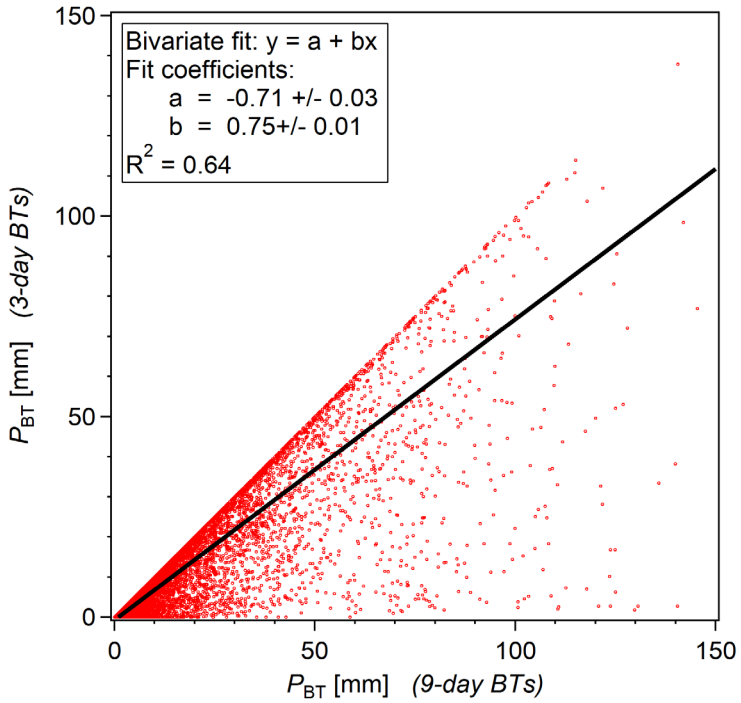

Figure S6. Scatter plot of cumulative precipitation, P_{BT}, (daily averages) along 3-day vs. 9-day back trajectories. Trajectories within the time period from 01 Jan 2014 to 31 Dec 2014 are analyzed here. Comparison shows that (on average) 75 % of the rain that the transported air parcels receive occurs during the last three days on their way to ATTO.

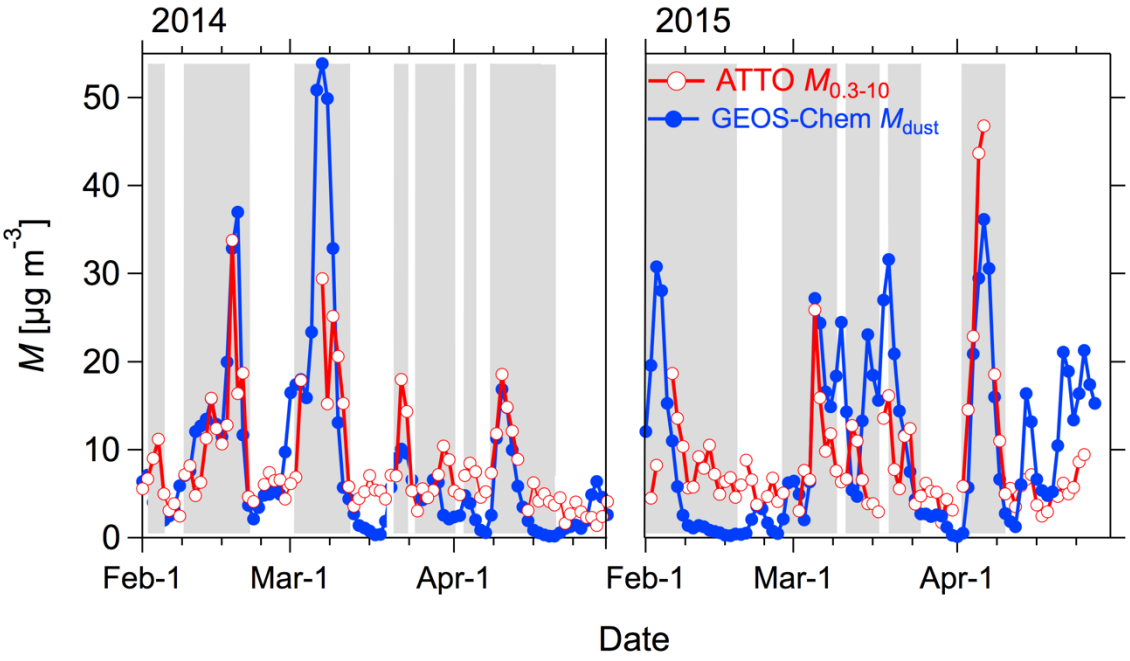

Figure S7. Comparison of experimental aerosol masses $M_{0.3\text{-}10}$ measured at the ATTO site and GEOS-Chem model calculation of the mass M_{dust} of dust aerosols being advected to the ATTO site. The comparison has been conducted for the wet season months Feb to May for the years 2014 and 2015. The LRT episodes as listed in Table 1 are shown as grey vertical shading. Note that M_{dust} represents dust aerosols only. Accordingly, M_{dust} approaches zero during clean episodes, whereas elevated $M_{0.3\text{-}10}$ levels during same time correspond to the background of PBAP.

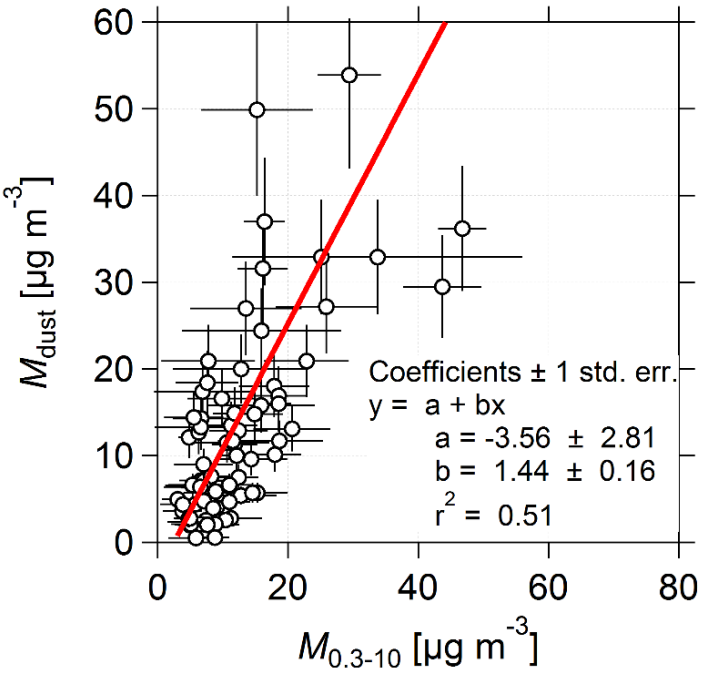

Figure S8. Scatter plot of measured aerosol mass concentration $M_{0.3\text{-}10}$ vs. GEOS-Chem model calculation of advected dust aerosol mass concentration M_{dust} according to Fig. S6. The red line represents a linear bivariate regression fit according to Cantrell (2008). The error bars in $M_{0.3\text{-}10}$ represent one standard deviation and in M_{dust} assuming an uncertainty of 20 %.

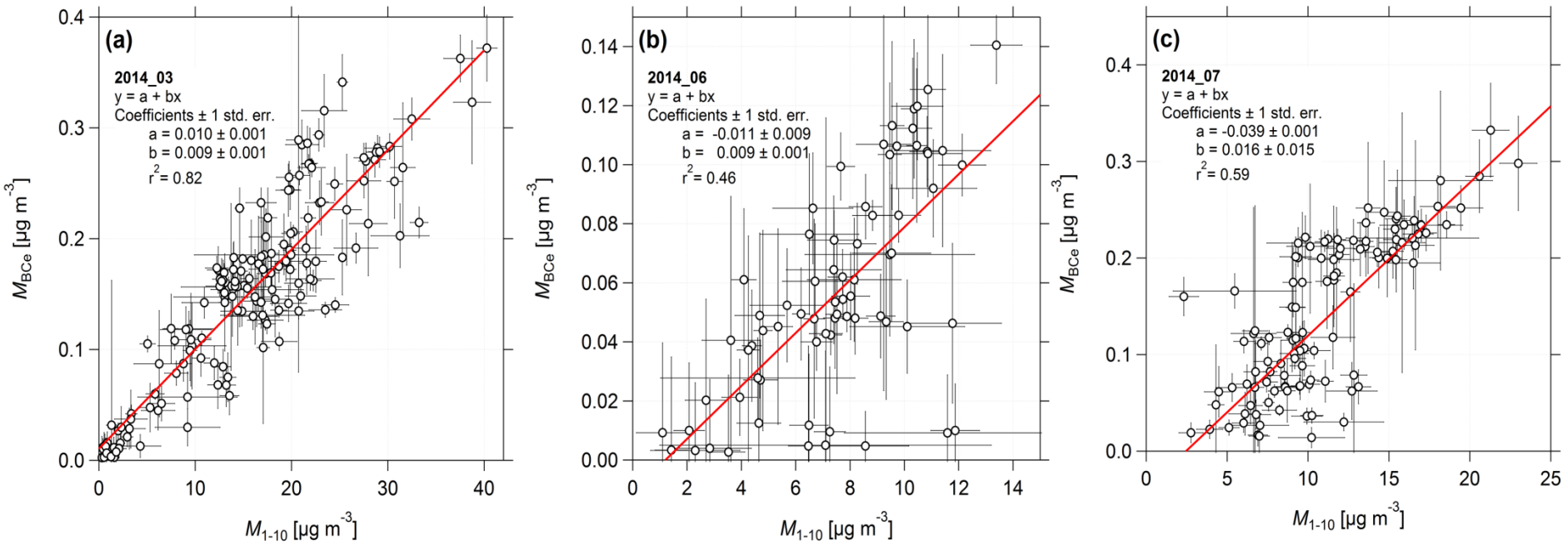

Figure S9. Scatter plots of coarse mode aerosol mass concentration, $M_{1\text{-}10}$, vs. BC_e mass concentration, M_{BCe}, for selected LRT episodes in 2014 (i.e., 2014_3, 2014_6, 2014_7, see Table 1). The red lines represents linear bivariate regression fits according to Cantrell (2008). The error bars in $M_{1\text{-}10}$ and M_{BCe} represent one standard deviation.

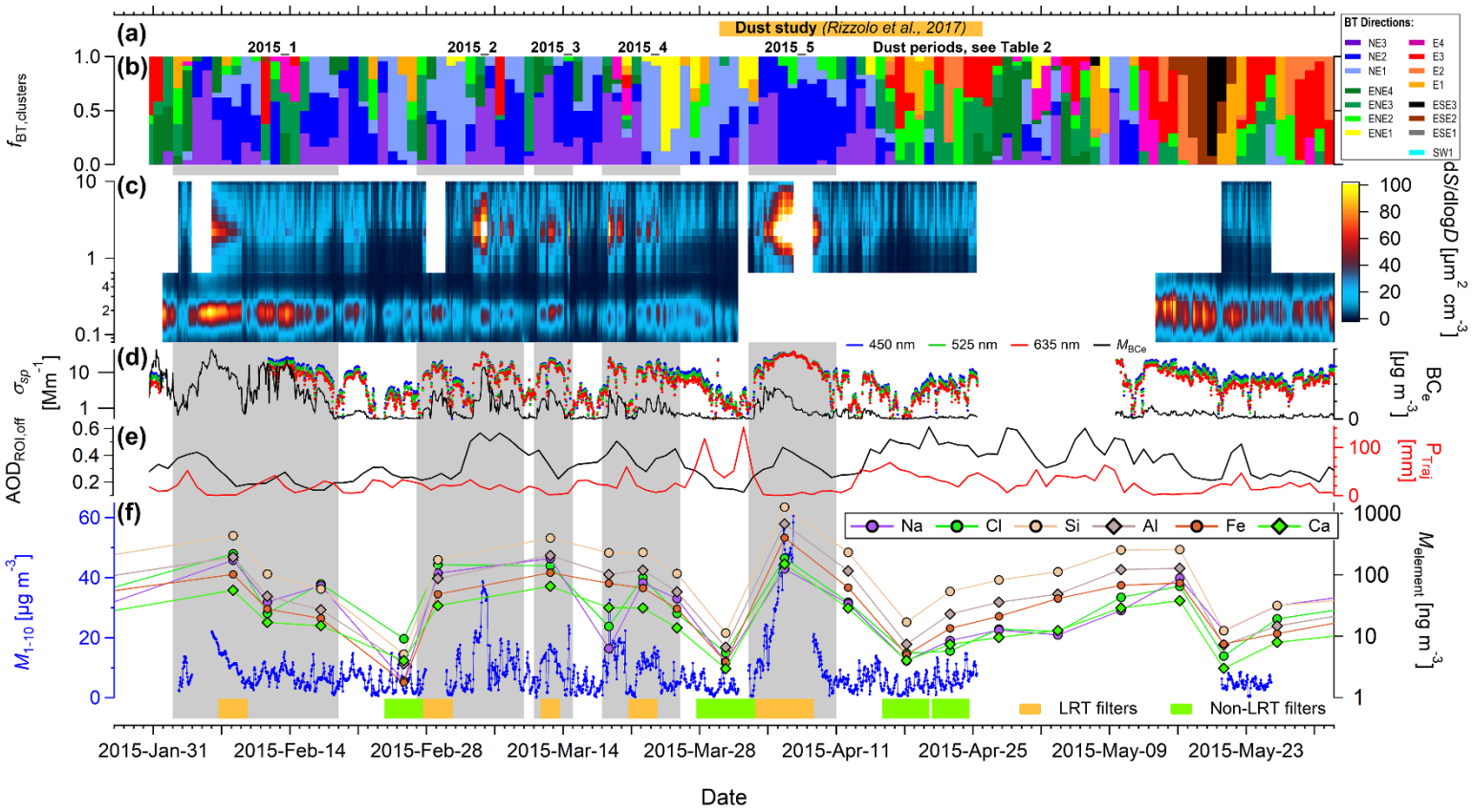

Figure S10. Overview of wet season months 2015 where: (**a**) Colored marker highlights an ATTO study by Rizzolo et al. (2016), investigating the impact of bioavailable iron as fertilizer for the Amazon rain forest, transported with African dust. (**b**) Frequency of occurrence, $f_{BT,\ clusters}$, of 15 back trajectory clusters as displayed in Fig. S4 (with identical cluster color coding). (**c**) Image plot of aerosol size surface distribution for size range from 80 nm to 10 µm. Note that the pronounced LRT pulse from 02 to 10 April 2015 (2015_5 event, Table 1) represents one of the strongest LRT events observed at ATTO in the context of this study. (**d**, left axis) Time series of the aerosol scattering coefficients, σ_{sp}, at three different wavelengths. (**d**, right axis) Black carbon mass concentration, M_{BCe}, with a corrected mass absorption cross section MAC of 11.4 $m^2\ g^{-1}$ during the wet season and 12.3 $m^2\ g^{-1}$ during the dry season. (**e**, left axis) Satellite-retrieved aerosol optical depth at 550 nm, area-averaged over the offshore region of interest (ROI_{off}, see Fig. S4). The $AOD_{ROI,off}$ time series represents the average of the MODIS data sets from the satellites Aqua and Terra. (**e**, right axis) HYSPLIT-retrieved accumulated precipitation, P_{BT}, along the trajectory tracks. (**f**, left axis) Aerosol

mass concentrations in the coarse mode 1-10 µm ($M_{1\text{-}10}$). (**f**, right axis) Total mass concentrations of selected elements based on EDXRF analysis, collected at the neighboring ZF2 site, which on average receives similar air masses that the ATTO site (Saturno et al., 2017). Selected LRT and non-LRT filters (which are marked in the bottom part of the figure as orange and green shading) were used for the more detailed analysis in Fig. 14 and Table S2. Due to comparatively long sampling times (3-7 days), the fine structure of the episodic LRT events was not captured by the time series on the aerosol chemical composition. However, the overall trends in $M_{1\text{-}10}$ and the elemental data in Fig. 18f agree well: The concentrations of characteristic dust marker elements (i.e., Si, Al, Ca, and Fe) as well as elements representing sea salt (i.e., Na and Cl) show clear increases during the LRT periods, which is particularly pronounced for the event 2015_5. Grey vertical bands mark episodes when Saharan LRT aerosol was measured at the ATTO site (see Table 1).

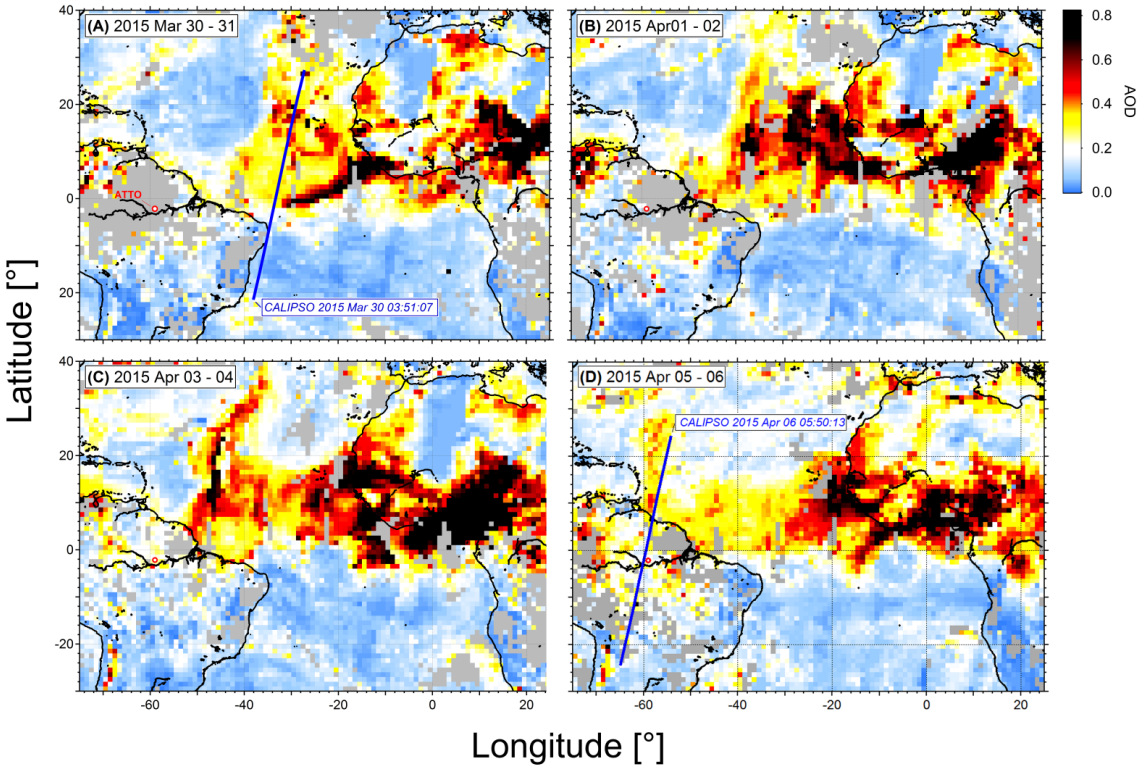

Figure S11. MODIS-derived AOD data showing Saharan dust outbreak, transatlantic passage, and intrusion into the Amazon Basin in early April 2015. Selected orbits of the CALIPSO spacecraft on 30 March and 06 April are shown in (**a**) and (**d**). Corresponding CALIOP lidar profiles transecting the dust plume are displayed in Fig. S11. The first panel for 30-31 March shows a particularly large plume in a latitude band between 40° N and the equator with the largest AOD values at its north and south boundaries. In the course of the following days, the plume travels further to the west reaching the Caribbean islands, Latin America, and finally also the ATTO region on 03 April. Note that large amounts of aerosol are constantly emitted from the Saharan and Sahel regions during the entire period. Accordingly, a heterogeneous mixing of dust and pyrogenic aerosols at large horizontal scales – as observed in the variable M_{BCe} and $M_{1\text{-}10}$ ratio – can plausibly be assumed. The gray areas represent pixels with no satellite data for the corresponding time periods.

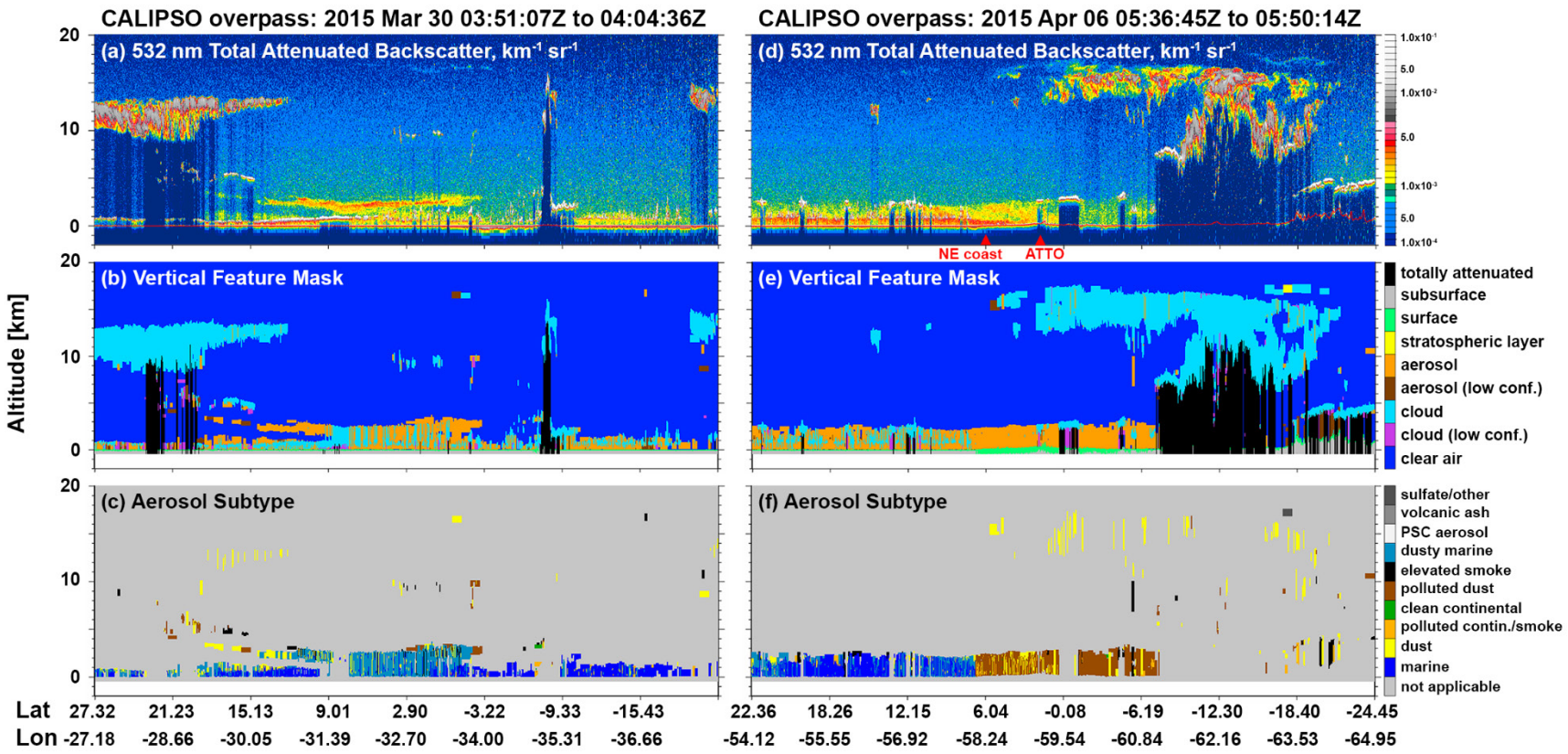

Figure S12. CALIPSO-derived lidar profiles of the African dust plume from March 30 and April 06 2015. The corresponding satellite orbits are shown as overlay with the MODIS AOD maps in Fig. S10. The first overpass (Fig S11a, b, and c) illustrates the dust outbreak at an early state over the Atlantic. Attenuated backscatter data indicate a lofted aerosol layer at 2-3 km altitude, which is clearly separated from the underlying layers at the north and south edges. The second lidar profile was recorded during an overpass directly above the ATTO region on 06 April close to the observed peak mass concentrations (Fig S11d, e, and f). Above the ATTO site, the vertical profile shows an approximately 3 km high and compact aerosol layer which is reaching to the ground. Albeit all uncertainties in the aerosol subtype classification, the lidar measurements also indicate a heterogeneous mixture of polluted and less polluted dust.

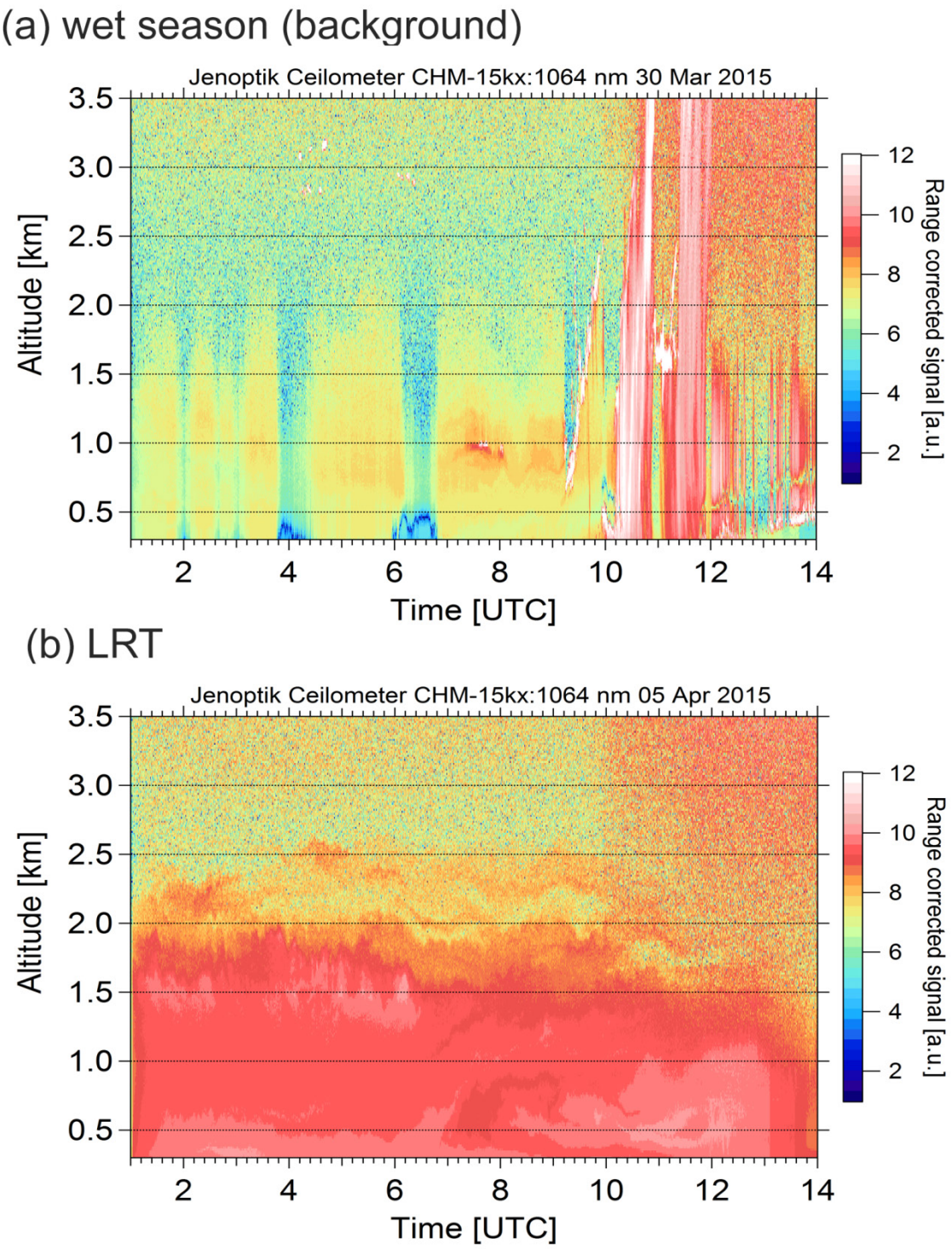

Figure S13. Temporal development of the range-corrected signal of the ceilometer Jenoptik CHM-15kx, on (a) Mar 30 (e.g. near background conditions); and (b) April 5 2015 (e.g., LRT episode) from 01:00-14:00 UTC at ATTO. The data have a temporal resolution of 30 s and vertical resolution of 15 m. During the LRT episode, a dust layer is visible at 2 km, persisting from the morning until early afternoon.

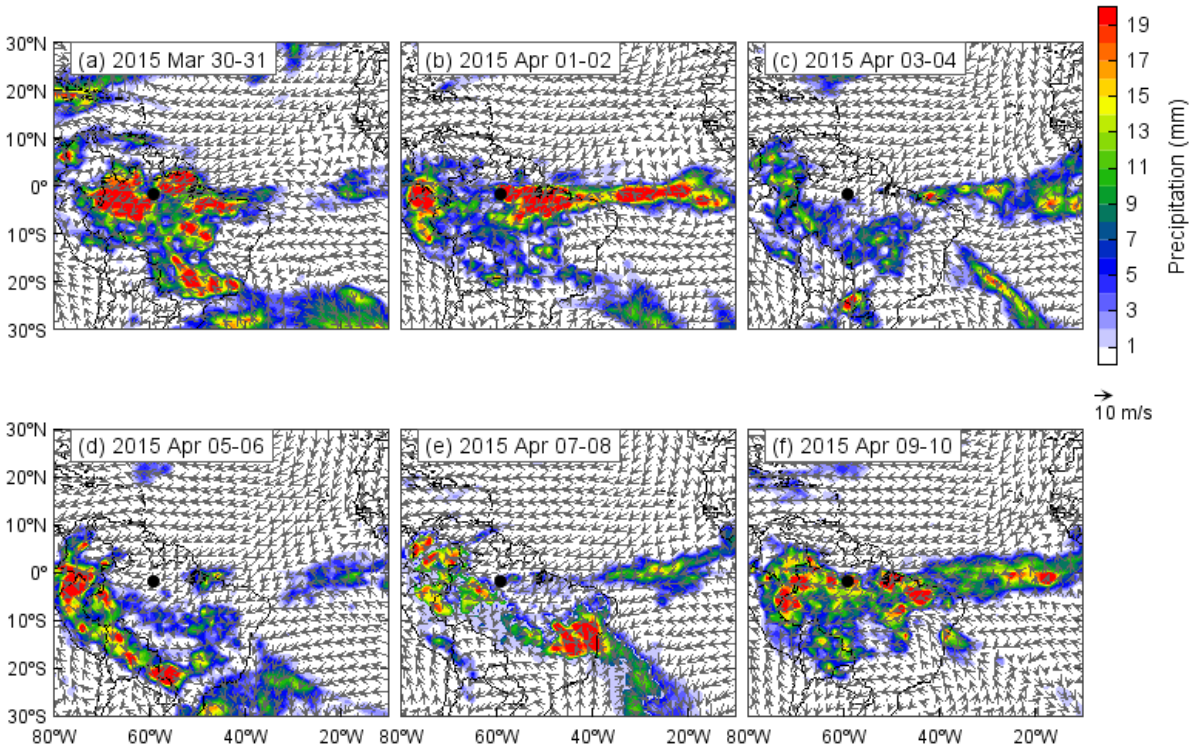

Figure S14. Wind data and precipitation daily averages from NCEP reanalysis data at a spatial resolution of 2.5 degrees from 02 to 13 April 2014, corresponding to 2015_5 period shown in Fig S10.

S4 Supplementary tables

Table S1. Densities of different coarse mode aerosol particle types as reported in the literature.

Compound / Aerosol type	Density [g cm^{-3}]	Reference	Comments
Pollen (angiospermae and gymnospermae)	0.82 ± 0.28	(Gregory, 1973)	Mean ± one standard deviation of all angiospermae and gymnospermae reported in Gregory 1973
Corn pollen	1.14 ± 0.05	(van Hout and Katz, 2004)	Density ± absolute error
Ragweed pollen	0.82 - 1.28	(Harrington and Metzger, 1963)	Mean value 1.27 at 75% RH
Fungal spores	1.10 ± 0.22	(Gregory, 1973)	Mean ± one standard deviation of all fungal spores reported in Gregory 1973
Conidia	1.08	(Sawyer et al., 1994)	Average of four species
Mineral and soil composition	2.2	(Renard et al., 2016)	According to Renard et al. 2016 compromise for common mineral particles: compact sand (2.1 g cm^{-3}), quartz (2.7 g cm^{-3}), limestone (2.5 g cm^{-3}), and silicon (2.3 g cm^{-3}).
Carbonaceous particles	1.4	(Renard et al., 2016)	--
Bacteria	1.1 - 1.2	(Jin-Bi et al., 2016)	Bacterial communities cultivated under laboratory conditions. Cell sizes 1-10 µm.

Table S2. Statistical distribution of the box and whisker plot, descriptive statistic (minimum, lower Q1, median, Q3, maximun) of total aerosol number concentration (> 4 nm, CPC derived), BC_e mass concentration, M_{BCe}, aerosol number concentration in the size range 0.3-1 µm, aerosol mass concentration in the size range 0.3-1 µm, aerosol number concentration in the size range 1-10 µm, and aerosol mass concentration in the size range 1-10 µm. Wet season, LRT episodes, transition periods and dry season from the Fig. 5.

Aerosol Number concentrations	density (g cm-3)	$N_{0.3-1}$ [cm $^{-3}$]					N_{1-10} [cm $^{-3}$]					N_{total} [cm $^{-3}$]				
		min	Q1	median	Q3	max	min	Q1	median	Q3	max	min	Q1	median	Q3	max
Wet	1.0	0.0	2.4	5.0	8.5	17.5	0.0	0.2	0.3	0.5	1.0	0.0	197	283	420	753
Dust		0.0	7.5	15.8	28.1	58.9	0.0	0.6	1.5	2.8	6.2	0.0	197	286	390	680
Transition		0.0	9.1	15.2	26.1	51.6	0.0	0.4	0.7	1.0	1.8	0.0	448	663	963	1730
Dry		0.1	37.5	57.8	87.0	161.2	0.0	0.8	1.1	1.4	2.4	0.0	1021	1337	1776	2901
Annual		**0.1**	**56.6**	**93.7**	**149.7**	**289.4**	**0.0**	**2.1**	**3.6**	**5.8**	**11.4**	**0.0**	**1863**	**2569**	**3549**	**6064**
Aerosol Mass concentrations	**density (g cm-3)**	**$M_{0.3-1}$ [µg m $^{-3}$]**					**M_{1-10} [µg m $^{-3}$]**					**M_{BCe} [µg m $^{-3}$]**				
		min	**Q1**	**median**	**Q3**	**max**	**min**	**Q1**	**median**	**Q3**	**max**	**min**	**Q1**	**median**	**Q3**	**max**
Wet	1.0	0.0	0.1	0.2	0.3	0.6	0.0	2.2	3.5	5.4	10.1	0.00	0.01	0.02	0.04	0.08
Dust		0.0	0.3	0.6	1.1	2.4	0.0	5.2	9.1	14.2	27.6	0.00	0.05	0.14	0.24	0.53
Transition		0.0	0.3	0.5	0.8	1.5	0.0	3.4	4.9	6.5	11.1	0.00	0.05	0.10	0.20	0.42
Dry		0.0	1.1	1.6	2.5	4.5	0.5	4.9	6.4	7.8	12.2	0.00	0.21	0.30	0.46	0.83
Annual		**0.0**	**1.7**	**2.9**	**4.6**	**9.0**	**0.5**	**15.7**	**23.8**	**33.9**	**61.1**	**0.00**	**0.32**	**0.56**	**0.94**	**1.86**

Table S3. Mean relative mass fractions, $f_{element}$, and elemental mass concentrations, $M_{element}$, of aerosol particles in size fractions 2.5 to 10 µm and <2.5 µm for LRT episodes vs. periods without LRT influence (called non-LRT here). All data points below the elemental detection limits were omitted in this analysis. The sampling periods of the 5 LRT filters and the 4 non-LRT filters are specified in Sect. 2.4 and plotted in Fig. S9. The average elemental fractions are quantified relative to the average deposited mass on the LRT vs. non-LRT filters, respectively. The data summarized here has been plotted in Fig. 14.

Element	Detection limit	LRT pulses						Absence of LRT pulses					
		<2.5 µm		>2.5 µm		total		<2.5 µm		>2.5 µm		total	
	[ng m^{-3}]	$M_{element}$ [ng m^{-3}]	$f_{element}$ [%]	$M_{element}$ [ng m^{-3}]	$f_{element}$ [%]	$M_{element}$ [ng m^{-3}]	$f_{element}$ [%]	$M_{element}$ [ng m^{-3}]	$f_{element}$ [%]	$M_{element}$ [ng m^{-3}]	$f_{element}$ [%]	$M_{element}$ [ng m^{-3}]	$f_{element}$ [%]
Na	28.00	50	2.2	81	1.2	130	1.4	--	--	--	--	--	--
Mg	29.00	31	1.3	71	1.1	100	1.1	--	--	--	--	--	--
Al	6.50	110	4.4	150	2.3	260	2.8	14	2.4	9.4	0.3	23	0.7
Si	6.50	210	8.8	290	4.4	500	5.5	18	3.3	17	0.6	35	1.1
P	3.00	4.4	0.2	16	0.2	20	0.2	--	--	11	0.4	11	0.3
S	3.40	150	6.2	46	0.7	190	2.1	29	5.1	8.4	0.3	37	1.1
Cl	2.00	2.1	0.1	160	2.3	160	1.7	2.2	0.4	3.4	0.1	5.6	0.2
K	1.60	72	3.0	93	1.4	170	1.8	7.0	1.2	28	1.0	35	1.0
Ca	3.30	19	0.8	47	0.7	66	0.7	--	--	4.0	0.1	4.0	0.1
Ti	2.10	7.0	0.3	12	0.2	19	0.2	--	--	--	--	--	--
Mn	1.50	1.9	0.1	5.2	0.1	7.1	0.1	--	--	--	--	--	--
Fe	2.10	51	2.1	93	1.4	140	1.6	4.2	0.8	4.1	0.1	8.3	0.3
Total mass [ng m^{-3}]	--	2390	--	6690	--	9090	--	560	--	2780	--	3340	--

Table S4. Seasonally averaged aerosol number size distributions, d*N*dlog*D*, for conditions during wet season, LRT episodes, transition periods, and dry season. The median d*N*dlog*D* values shown here are those that are plotted in Fig. 6a in the main text. The diameters, *D*, correspond to the geometric mean of OPS bin definitions.

***D* [µm]**	**d*N*dlog*D* [cm^{-3}]**			
	wet	**LRT**	**trans**	**dry**
0.34	39.32	106.96	131.7	473.28
0.42	7.02	21.5	24.47	102.76
0.52	2.37	9.77	6.96	18.7
0.66	1.12	5.2	3.01	6.31
0.82	0.81	4.26	2.1	4.14
1.08	0.48	2.92	1.3	2.37
1.38	0.49	2.68	1.37	2.52
1.60	0.56	2.96	1.66	3.05
1.93	0.57	2.57	1.24	2.05
2.41	0.49	1.48	0.74	0.92
3.00	0.32	0.8	0.39	0.45
3.73	0.18	0.42	0.22	0.25
4.64	0.09	0.18	0.1	0.12
5.78	0.04	0.07	0.05	0.06
7.20	0.02	0.03	0.03	0.03
8.96	0.01	0.01	0.01	0.02

Table S5. Seasonally averaged aerosol surface size distributions, d*S*dlog*D*, for conditions during wet season, LRT episodes, transition periods, and dry season. The median d*S*dlog*D* values shown here are those that are plotted in Fig. 6b in the main text. The diameters, *D*, correspond to the geometric mean of OPS bin definitions.

***D* [µm]**	**d*S*dlog*D* [µm^2 cm^{-3}]**			
	wet	**LRT**	**trans**	**dry**
0.34	14.03	38.16	46.99	168.85
0.42	3.88	11.89	13.53	56.81
0.52	2.03	8.36	5.96	16.01
0.66	1.53	7.1	4.12	8.62
0.82	1.7	9	4.45	8.74
1.08	1.81	10.94	4.87	8.88
1.38	2.91	16.03	8.2	15.06
1.60	4.53	23.9	13.37	24.68
1.93	6.8	30.49	14.75	24.32
2.41	8.97	27.32	13.64	16.98
3.00	8.99	22.69	11.27	12.87
3.73	8.04	18.53	9.77	10.91
4.64	6.01	12.58	7.19	8.17
5.78	4.11	7.53	4.95	5.93
7.20	3.42	5.63	4.49	5.57
8.96	2.2	3.5	3.39	4.59

Table S6. Seasonally averaged aerosol volume size distributions, dVdlog$D$, for conditions during wet season, LRT episodes, transition periods, dry season, and 'LRT – wet' conditions. The median dVdlog$D$ values shown here are those that are plotted in Fig. 6c and d in the main text. The diameters, D, correspond to the geometric mean of OPS bin definitions.

D [µm]	dVdlog$D$ [µm^3 cm^{-3}]				
	wet	LRT	trans	dry	LRT-wet
0.34	0.79	2.14	2.64	9.48	1.36
0.42	0.27	0.83	0.95	3.97	0.56
0.52	0.18	0.73	0.52	1.39	0.55
0.66	0.17	0.78	0.45	0.95	0.61
0.82	0.23	1.23	0.61	1.19	1.00
1.08	0.33	1.99	0.89	1.62	1.66
1.38	0.67	3.69	1.89	3.46	3.02
1.60	1.21	6.39	3.57	6.59	5.18
1.93	2.20	9.88	4.78	7.88	7.67
2.41	3.62	11.02	5.50	6.85	7.40
3.00	4.52	11.40	5.66	6.47	6.88
3.73	5.03	11.59	6.11	6.82	6.56
4.64	4.68	9.80	5.60	6.37	5.12
5.78	3.98	7.30	4.80	5.75	3.32
7.20	4.12	6.80	5.42	6.73	2.67
8.96	3.31	5.26	5.09	6.89	1.95

Table S7. Aerosol mass size distribution, dMdlog$D$, from CLAIRE-98 experiment in Balbina, Brazil, representing conditions during African dust advection. Data is plotted in Fig. 6d in the main text and details can be found in Formenti et al. (2001) as well as Sect. 3.2 of the present work.

D [µm]	dVdlog$D$ [µm^3 cm^{-3}] LRT - wet
0.07	0.02
0.12	0.04
0.19	0.08
0.29	0.24
0.47	0.59
0.69	1.12
0.93	3.04
1.36	8.19
2.17	12.47
3.38	10.82
6.29	7.74
11.75	0.65

References

Abouchami, W., Näthe, K., Kumar, A., Galer, S. J. G., Jochum, K. P., Williams, E., Horbe, A. M. C., Rosa, J. W. C., Balsam, W., Adams, D., Mezger, K., and Andreae, M. O.: Geochemical and isotopic characterization of the Bodélé Depression dust source and implications for transatlantic dust transport to the Amazon Basin, Earth and Planetary Science Letters, 380, 112-123, https://doi.org/10.1016/j.epsl.2013.08.028, 2013.

Andreae, M. O.: Soot Carbon and Excess Fine Potassium: Long-Range Transport of Combustion-Derived Aerosols, Science, 220, 1148, 1983.

Andreae, M. O., Acevedo, O. C., Araùjo, A., Artaxo, P., Barbosa, C. G. G., Barbosa, H. M. J., Brito, J., Carbone, S., Chi, X., Cintra, B. B. L., da Silva, N. F., Dias, N. L., Dias-Júnior, C. Q., Ditas, F., Ditz, R., Godoi, A. F. L., Godoi, R. H. M., Heimann, M., Hoffmann, T., Kesselmeier, J., Könemann, T., Krüger, M. L., Lavric, J. V., Manzi, A. O., Moran-Zuloaga, D., Nölscher, A. C., Santos Nogueira, D., Piedade, M. T. F., Pöhlker, C., Pöschl, U., Rizzo, L. V., Ro, C. U., Ruckteschler, N., Sá, L. D. A., Sá, M. D. O., Sales, C. B., Santos, R. M. N. D., Saturno, J., Schöngart, J., Sörgel, M., de Souza, C. M., de Souza, R. A. F., Su, H., Targhetta, N., Tóta, J., Trebs, I., Trumbore, S., van Eijck, A., Walter, D., Wang, Z., Weber, B., Williams, J., Winderlich, J., Wittmann, F., Wolff, S., and Yáñez-Serrano, A. M.: The Amazon Tall Tower Observatory (ATTO) in the remote Amazon Basin: overview of first results from ecosystem ecology, meteorology, trace gas, and aerosol measurements, Atmos. Chem. Phys., 15, 10723-10776, https://doi.org/10.5194/acp-15-10723-2015, 2015.

Andreae, M. O., Afchine, A., Albrecht, R., Holanda, B. A., Artaxo, P., Barbosa, H. M. J., Borrmann, S., Cecchini, M. A., Costa, A., Dollner, M., Fütterer, D., Järvinen, E., Jurkat, T., Klimach, T., Konemann, T., Knote, C., Krämer, M., Krisna, T., Machado, L. A. T., Mertes, S., Minikin, A., Pöhlker, C., Pöhlker, M. L., Pöschl, U., Rosenfeld, D., Sauer, D., Schlager, H., Schnaiter, M., Schneider, J., Schulz, C., Spanu, A., Sperling, V. B., Voigt, C., Walser, A., Wang, J., Weinzierl, B., Wendisch, M., and Ziereis, H.: Aerosol characteristics and particle production in the upper troposphere over the Amazon Basin, Atmos. Chem. Phys., 18, 921-961, 10.5194/acp-18-921-2018, 2018.

Andreae, M. O., Artaxo, P., Beck, V., Bela, M., Freitas, S., Gerbig, C., Longo, K., Munger, J. W., Wiedemann, K. T., and Wofsy, S. C.: Carbon monoxide and related trace gases and aerosols over the Amazon Basin during the wet and dry seasons, Atmospheric Chemistry and Physics, 12, 6041-6065, 10.5194/acp-12-6041-2012, 2012.

Andreae, M. O., Berresheim, H., Bingemer, H., Jacob, D. J., Lewis, B. L., Li, S. M., and Talbot, R. W.: The atmospheric sulfur cycle over the Amazon Basin: 2. Wet season, Journal of Geophysical Research: Atmospheres, 95, 16813-16824, 10.1029/JD095iD10p16813, 1990a.

Andreae, M. O., Charlson, R. J., Bruynseels, F., Storms, H., Van Grieken, R., and Maenhaut, W.: Internal Mixture of Sea Salt, Silicates, and Excess Sulfate in Marine Aerosols, Science, 232, 1620-1623, 1986.

Andreae, M. O., Talbot, R. W., Berresheim, H., and Beecher, K. M.: Precipitation chemistry in central Amazonia, Journal of Geophysical Research: Atmospheres, 95, 16987-16999, 10.1029/JD095iD10p16987, 1990b.

Artaxo, P., Gerab, F., and Rabello, M. L. C.: Elemental composition of aerosol-particles from 2 atmospheric monitoring stations in the Amazon basin, Nucl. Instrum. Methods Phys. Res. Sect. B-Beam Interact. Mater. Atoms, 75, 277-281, 10.1016/0168-583x(93)95658-r, 1993.

Baars, H., Ansmann, A., Althausen, D., Engelmann, R., Artaxo, P., Pauliquevis, T., and Souza, R.: Further evidence for significant smoke transport from Africa to Amazonia, Geophysical Research Letters, 38, 6, 10.1029/2011gl049200, 2011.

Baker, A. R., Lesworth, T., Adams, C., Jickells, T. D., and Ganzeveld, L.: Estimation of atmospheric nutrient inputs to the Atlantic Ocean from 50°N to 50°S based on large-scale field sampling: Fixed nitrogen and dry deposition of phosphorus, Glob. Biogeochem. Cycle, 24, n/a-n/a, 10.1029/2009GB003634, 2010.

Barbosa, P. M., Stroppiana, D., Gregoire, J. M., and Pereira, J. M. C.: An assessment of vegetation fire in Africa (1981-1991): Burned areas, burned biomass, and atmospheric emissions, Global Biogeochemical Cycles, 13, 933-950, 10.1029/1999gb900042, 1999.

Baron, P. A., Mazumder, M. K., Cheng, Y.-S., and Peters, T. M.: Real-Time Techniques for Aerodynamic Size Measurement, in: Aerosol Measurement, John Wiley & Sons, Inc., 313-338, 2011.

Ben-Ami, Y., Koren, I., and Altaratz, O.: Patterns of North African dust transport over the Atlantic: winter vs. summer, based on CALIPSO first year data, Atmospheric Chemistry and Physics, 9, 7867-7875, 2009.

Ben-Ami, Y., Koren, I., Rudich, Y., Artaxo, P., Martin, S. T., and Andreae, M. O.: Transport of North African dust from the Bodélé depression to the Amazon Basin: a case study, Atmos. Chem. Phys., 10, 7533-7544, 10.5194/acp-10-7533-2010, 2010.

Bristow, C. S., Hudson-Edwards, K. A., and Chappell, A.: Fertilizing the Amazon and equatorial Atlantic with West African dust, Geophysical Research Letters, 37, 5, 10.1029/2010gl043486, 2010.

Brito, J., Rizzo, L. V., Morgan, W. T., Coe, H., Johnson, B., Haywood, J., Longo, K., Freitas, S., Andreae, M. O., and Artaxo, P.: Ground-based aerosol characterization during the South American Biomass Burning Analysis (SAMBBA) field experiment, Atmospheric Chemistry and Physics, 14, 12069-12083, 10.5194/acp-14-12069-2014, 2014.

Brown, J. K. M., and Hovmøller, M. S.: Aerial Dispersal of Pathogens on the Global and Continental Scales and Its Impact on Plant Disease, Science, 297, 537, 2002.

Cantrell, C. A.: Technical Note: Review of methods for linear least-squares fitting of data and application to atmospheric chemistry problems, Atmos. Chem. Phys., 8, 5477-5487, 10.5194/acp-8-5477-2008, 2008.

Chen, Q., Farmer, D. K., Rizzo, L. V., Pauliquevis, T., Kuwata, M., Karl, T. G., Guenther, A., Allan, J. D., Coe, H., Andreae, M. O., Pöschl, U., Jimenez, J. L., Artaxo, P., and Martin, S. T.: Submicron particle mass concentrations and sources in the Amazonian wet season (AMAZE-08), Atmos. Chem. Phys., 15, 3687-3701, 10.5194/acp-15-3687-2015, 2015.

Chen, Q., Farmer, D. K., Schneider, J., Zorn, S. R., Heald, C. L., Karl, T. G., Guenther, A., Allan, J. D., Robinson, N., Coe, H., Kimmel, J. R., Pauliquevis, T., Borrmann, S., Pöschl, U., Andreae, M. O., Artaxo, P., Jimenez, J. L., and Martin, S. T.: Mass spectral characterization of submicron biogenic organic particles in the Amazon Basin, Geophysical Research Letters, 36, n/a-n/a, 10.1029/2009GL039880, 2009.

Choobari, O. A., Zawar-Reza, P., and Sturman, A.: The global distribution of mineral dust and its impacts on the climate system: A review, Atmospheric Research, 138, 152-165, http://dx.doi.org/10.1016/j.atmosres.2013.11.007, 2014.

Darwin, C.: An account of the Fine Dust which often falls on Vessels in the Atlantic Ocean, Quarterly Journal of the Geological Society, 2, 26, 1846.

Després, V. R., Huffman, J. A., Burrows, S. M., Hoose, C., Safatov, A. S., Buryak, G., Fröhlich-Nowoisky, J., Elbert, W., Andreae, M. O., Pöschl, U., and Jaenicke, R.: Primary biological aerosol particles in the atmosphere: a review, 2012, 64, 10.3402/tellusb.v64i0.15598, 2012.

Di Biagio, C., Formenti, P., Balkanski, Y., Caponi, L., Cazaunau, M., Pangui, E., Journet, E., Nowak, S., Caquineau, S., Andreae, M. O., Kandler, K., Saeed, T., Piketh, S., Seibert, D., Williams, E., and Doussin, J. F.: Global scale variability of the mineral dust long-wave refractive index: a new dataset of in situ measurements for climate modeling and remote sensing, Atmos. Chem. Phys., 17, 1901-1929, 10.5194/acp-17-1901-2017, 2017.

Du, R., Du, P., Lu, Z., Ren, W., Liang, Z., Qin, S., Li, Z., Wang, Y., and Fu, P.: Evidence for a missing source of efficient ice nuclei, Nature, 7, 39673, 10.1038/srep39673, https://www.nature.com/articles/srep39673#supplementary-information, 2017.

Dudley, R., Kaspari, M., and Yanoviak, S. P.: Lust for Salt in the Western Amazon, Biotropica, 44, 6-9, 10.1111/j.1744-7429.2011.00818.x, 2012.

Dusek, U., Frank, G. P., Hildebrandt, L., Curtius, J., Schneider, J., Walter, S., Chand, D., Drewnick, F., Hings, S., Jung, D., Borrmann, S., and Andreae, M. O.: Size matters more than chemistry for cloud-nucleating ability of aerosol particles, Science, 312, 1375-1378, 10.1126/science.1125261, 2006.

Ehrenberg, C. G.: Passatstaub und Blutregen. Ein Großes Organisches Unsichtbares Wirken und Leben in Des Atmosphäre. - Primary Source Edition, BiblioLife, 1849.

Engelstaedter, S., Washington, R., and Mahowald, N.: Impact of changes in atmospheric conditions in modulating summer dust concentration at Barbados: A back-trajectory analysis, J. Geophys. Res.-Atmos., 114, 20, 10.1029/2008jd011180, 2009.

Formenti, P., Andreae, M. O., Lange, L., Roberts, G., Cafmeyer, J., Rajta, I., Maenhaut, W., Holben, B. N., Artaxo, P., and Lelieveld, J.: Saharan dust in Brazil and Suriname during the Large-Scale Biosphere-Atmosphere Experiment in Amazonia (LBA) - Cooperative LBA Regional Experiment (CLAIRE) in March 1998, Journal of Geophysical Research-Atmospheres, 106, 14919-14934, 10.1029/2000jd900827, 2001.

Formenti, P., Schütz, L., Balkanski, Y., Desboeufs, K., Ebert, M., Kandler, K., Petzold, A., Scheuvens, D., Weinbruch, S., and Zhang, D.: Recent progress in understanding physical and chemical properties of African and Asian mineral dust, Atmos. Chem. Phys., 11, 8231-8256, 10.5194/acp-11-8231-2011, 2011.

Fröhlich-Nowoisky, J., Kampf, C. J., Weber, B., Huffman, J. A., Pöhlker, C., Andreae, M. O., Lang-Yona, N., Burrows, S. M., Gunthe, S. S., Elbert, W., Su, H., Hoor, P., Thines, E., Hoffmann, T., Després, V. R., and Pöschl, U.: Bioaerosols in the Earth System: Climate, Health, and Ecosystem Interactions, Atmospheric Research, http://dx.doi.org/10.1016/j.atmosres.2016.07.018, 2016.

Fuchs, J., and Cermak, J.: Where Aerosols Become Clouds—Potential for Global Analysis Based on CALIPSO Data, Remote Sensing, 7, 4178, 2015.

Garrison, V. H., Majewski, M. S., Foreman, W. T., Genualdi, S. A., Mohammed, A., and Massey Simonich, S. L.: Persistent organic contaminants in Saharan dust air masses in West Africa, Cape Verde and the eastern Caribbean, Sci. Total Environ., 468–469, 530-543, http://dx.doi.org/10.1016/j.scitotenv.2013.08.076, 2014.

Gilbert, G. S., and Reynolds, D. R.: Nocturnal Fungi: Airborne Spores in the Canopy and Understory of a Tropical Rain Forest, Biotropica, 37, 462-464, 2005.

Gläser, G., Wernli, H., Kerkweg, A., and Teubler, F.: The transatlantic dust transport from North Africa to the Americas—Its characteristics and source regions, Journal of Geophysical Research: Atmospheres, 120, 11,231-211,252, 10.1002/2015JD023792, 2015.

Goudie, A. S.: Desert dust and human health disorders, Environment International, 63, 101-113, http://dx.doi.org/10.1016/j.envint.2013.10.011, 2014.

Graham, B., Guyon, P., Maenhaut, W., Taylor, P. E., Ebert, M., Matthias-Maser, S., Mayol-Bracero, O. L., Godoi, R. H. M., Artaxo, P., Meixner, F. X., Moura, M. A. L., Rocha, C. H. E. D. A., Grieken, R. V., Glovsky, M. M., Flagan, R. C., and Andreae, M. O.: Composition and diurnal variability of the natural Amazonian aerosol, Journal of Geophysical Research: Atmospheres, 108, n/a-n/a, 10.1029/2003JD004049, 2003.

Gregory, P. H.: The microbiology of the atmosphere, Bd. 1973,Teil 2, Wiley, 1973.

Harrington, J. B., and Metzger, K.: Ragweed Pollen Density, American Journal of Botany, 50, 532-539, 10.2307/2440028, 1963.

Hoose, C., Kristjánsson, J. E., and Burrows, S. M.: How important is biological ice nucleation in clouds on a global scale?, Environmental Research Letters, 5, 024009, 2010.

Huffman, J. A., Sinha, B., Garland, R. M., Snee-Pollmann, A., Gunthe, S. S., Artaxo, P., Martin, S. T., Andreae, M. O., and Pöschl, U.: Size distributions and temporal variations of biological aerosol particles in the Amazon rainforest characterized by microscopy and real-time UV-APS fluorescence techniques during AMAZE-08, Atmospheric Chemistry and Physics, 12, 11997-12019, 10.5194/acp-12-11997-2012, 2012.

Janhäll, S., Andreae, M. O., and Pöschl, U.: Biomass burning aerosol emissions from vegetation fires: particle number and mass emission factors and size distributions, Atmos. Chem. Phys., 10, 1427-1439, 10.5194/acp-10-1427-2010, 2010.

Jin-Bi, Z., Lei, D., Ying-Ping, W., Li, Z., Jin-Lei, W., Hai-Yang, Z., and Li, F.: Theoretical studies on particle shape classification based on simultaneous small forward angle light scattering and aerodynamic sizing, Chinese Physics B, 25, 034201, 2016.

Kalafut-Pettibone, A. J., Wang, J., Eichinger, W. E., Clarke, A., Vay, S. A., Blake, D. R., and Stanier, C. O.: Size-resolved aerosol emission factors and new particle formation/growth activity occurring in Mexico City during the MILAGRO 2006 Campaign, Atmos. Chem. Phys., 11, 8861-8881, 10.5194/acp-11-8861-2011, 2011.

Kanitz, T., Engelmann, R., Heinold, B., Baars, H., Skupin, A., and Ansmann, A.: Tracking the Saharan Air Layer with shipborne lidar across the tropical Atlantic, Geophys. Res. Lett., 41, 1044-1050, 10.1002/2013gl058780, 2014.

Kaufman, Y. J., Koren, I., Remer, L. A., Rosenfeld, D., and Rudich, Y.: The effect of smoke, dust, and pollution aerosol on shallow cloud development over the Atlantic Ocean, Proceedings of the National Academy of Sciences of the United States of America, 102, 11207-11212, 10.1073/pnas.0505191102, 2005.

Knippertz, P., Tesche, M., Heinold, B., Kandler, K., Toledano, C., and Esselborn, M.: Dust mobilization and aerosol transport from West Africa to Cape Verde—a meteorological overview of SAMUM-2, Tellus B, 63, 430-447, 10.1111/j.1600-0889.2011.00544.x, 2011.

Knippertz, P., and Todd, M. C.: Mineral dust aerosols over the Sahara: Meteorological controls on emission and transport and implications for modeling, Rev. Geophys., 50, n/a-n/a, 10.1029/2011RG000362, 2012.

Koren, I., Yoram, J. K., Richard, W., Martin, C. T., Yinon, R., Martins., J. V., and Daniel, R.: The Bodélé depression: a single spot in the Sahara that provides most of the mineral dust to the Amazon forest, Environmental Research Letters, 1, 014005, 2006.

Krejci, R., Strom, J., de Reus, M., Hoor, P., Williams, J., Fischer, H., and Hansson, H. C.: Evolution of aerosol properties over the rain forest in Surinam, South America, observed from aircraft during the LBA-CLAIRE 98 experiment, J. Geophys. Res.-Atmos., 108, 17, 10.1029/2001jd001375, 2003.

Kumar, A., Abouchami, W., Galer, S. J. G., Garrison, V. H., Williams, E., and Andreae, M. O.: A radiogenic isotope tracer study of transatlantic dust transport from Africa to the Caribbean, Atmospheric Environment, 82, 130-143, 10.1016/j.atmosenv.2013.10.021, 2014.

Kumar, A., Abouchami, W., Galer, S. J. G., Singh, S. P., Fomba, K. W., Prospero, J. M., and Andreae, M. O.: Seasonal radiogenic isotopic variability of the African dust outflow to the tropical Atlantic Ocean and across to the Caribbean, Earth and Planetary Science Letters, 487, 94-105, https://doi.org/10.1016/j.epsl.2018.01.025, 2018.

Liu, Z., Omar, A., Vaughan, M., Hair, J., Kittaka, C., Hu, Y., Powell, K., Trepte, C., Winker, D., Hostetler, C., Ferrare, R., and Pierce, R.: CALIPSO lidar observations of the optical properties of Saharan dust: A case study of long-range transport, Journal of Geophysical Research: Atmospheres, 113, n/a-n/a, 10.1029/2007JD008878, 2008.

Makowski Giannoni, S., Trachte, K., Rollenbeck, R., Lehnert, L., Fuchs, J., and Bendix, J.: Atmospheric salt deposition in a tropical mountain rainforest at the eastern Andean slopes of south Ecuador – Pacific or Atlantic origin?, Atmos. Chem. Phys., 16, 10241-10261, 10.5194/acp-16-10241-2016, 2016.

Martin, S. T., Andreae, M. O., Artaxo, P., Baumgardner, D., Chen, Q., Goldstein, A. H., Guenther, A., Heald, C. L., Mayol-Bracero, O. L., McMurry, P. H., Pauliquevis, T., Poschl, U., Prather, K. A., Roberts, G. C., Saleska, S. R., Dias, M. A. S., Spracklen, D. V., Swietlicki, E., and Trebs, I.: Sources and properties of the Amazonian aerosol particles, Rev. Geophys., 48, 42, 10.1029/2008rg000280, 2010.

Möhler, O., DeMott, P. J., Vali, G., and Levin, Z.: Microbiology and atmospheric processes: the role of biological particles in cloud physics, Biogeosciences, 4, 1059-1071, 2007.

Morris, C. E., Sands, D. C., Vinatzer, B. A., Glaux, C., Guilbaud, C., Buffiere, A., Yan, S., Dominguez, H., and Thompson, B. M.: The life history of the plant pathogen Pseudomonas syringae is linked to the water cycle, ISME J, 2, 321-334, 2008.

Okin, G. S., Baker, A. R., Tegen, I., Mahowald, N. M., Dentener, F. J., Duce, R. A., Galloway, J. N., Hunter, K., Kanakidou, M., Kubilay, N., Prospero, J. M., Sarin, M., Surapipith, V., Uematsu, M., and Zhu, T.: Impacts of atmospheric nutrient deposition on marine productivity: Roles of nitrogen, phosphorus, and iron, Glob. Biogeochem. Cycle, 25, n/a-n/a, 10.1029/2010GB003858, 2011.

Pauliquevis, T., Lara, L. L., Antunes, M. L., and Artaxo, P.: Aerosol and precipitation chemistry measurements in a remote site in Central Amazonia: the role of biogenic contribution, Atmospheric Chemistry and Physics, 12, 4987-5015, 10.5194/acp-12-4987-2012, 2012.

Pöhlker, C., Wiedemann, K. T., Sinha, B., Shiraiwa, M., Gunthe, S. S., Smith, M., Su, H., Artaxo, P., Chen, Q., Cheng, Y. F., Elbert, W., Gilles, M. K., Kilcoyne, A. L. D., Moffet, R. C., Weigand, M., Martin, S. T., Poeschl, U., and Andreae, M. O.: Biogenic Potassium Salt Particles as Seeds for Secondary Organic Aerosol in the Amazon, Science, 337, 1075-1078, 10.1126/science.1223264, 2012.

Pöhlker, C., Walter, D., Paulsen, H., Könemann, T., Rodríguez-Caballero, E., Moran-Zuloaga, D., Brito, J., Carbone, S., Degrendele, C., Després, V. R., Ditas, F., Holanda, B. A., Kaiser, J. W., Lammel, G., Lavrič, J. V., Jing, M., Pickersgill, D., Pöhlker, M. L., Praß, M., Ruckteschler, N., Saturno, J., Sörgel, M., Wang, Q., Weber, B., Wolff, S., Artaxo, P., Pöschl, U., and Andreae, M. O.: Land cover and its transformation in the backward trajectory footprint of the Amazon Tall Tower Observatory, Atmos. Chem. Phys. Diss, submitted, 2018.

Pöhlker, M. L., Pöhlker, C., Klimach, T., Hrabe de Angelis, I., Barbosa, H. M. J., Brito, J., Carbone, S., Cheng, Y., Chi, X., Ditas, F., Ditz, R., Gunthe, S. S., Kesselmeier, J., Könemann, T., Lavrič, J. V., Martin, S. T., Moran-Zuloaga, D., Rose, D., Saturno, J., Su, H., Thalman, R., Walter, D., Wang, J., Wolff, S., Artaxo, P., Andreae, M. O., and Pöschl, U.: Long-term observations of atmospheric aerosol, cloud condensation nuclei concentration and hygroscopicity in the Amazon rain forest – Part 1: Size-resolved characterization and new model parameterizations for CCN prediction, Atmos. Chem. Phys., 16, 15709-15740, https://doi.org/10.5194/acp-16-15709-2016, 2016.

Pöhlker, M. L., Pöhlker, C., Ditas, F., Klimach, T., Hrabe de Angelis, I., Araujo, A., Brito, J., Carbone, S., Chi, X., Cheng, Y., Ditz, R., Gunthe, S. S., Kesselmeier, J., Könemann, T., Lavric, J. V., Martin, S. T., Moran, D., Rose, D., Saturno, J., Su, H., Thalman, R., Walter, D., Wang, J., Wolff, S., Barbosa, H. M. J., Artaxo, P., Andreae, M. O., and Pöschl, U.: Long-term observations of cloud condensation nuclei in the Amazon rain forest – Part 2: Variability and characteristic differences under near-pristine, biomass burning, and long-range transport conditions, Atmos. Chem. Phys. Discuss., https://doi.org/10.5194/acp-2017-847, in review, 2017.

Pöschl, U., Martin, S. T., Sinha, B., Chen, Q., Gunthe, S. S., Huffman, J. A., Borrmann, S., Farmer, D. K., Garland, R. M., Helas, G., Jimenez, J. L., King, S. M., Manzi, A., Mikhailov, E., Pauliquevis, T., Petters, M. D., Prenni, A. J., Roldin, P., Rose, D., Schneider, J., Su, H., Zorn, S. R., Artaxo, P., and Andreae, M. O.: Rainforest Aerosols as Biogenic Nuclei of Clouds and Precipitation in the Amazon, Science, 329, 1513-1516, 10.1126/science.1191056, 2010.

Pöschl, U., and Shiraiwa, M.: Multiphase Chemistry at the Atmosphere–Biosphere Interface Influencing Climate and Public Health in the Anthropocene, Chemical Reviews, 115, 4440-4475, 10.1021/cr500487s, 2015.

Prenni, A. J., Petters, M. D., Kreidenweis, S. M., Heald, C. L., Martin, S. T., Artaxo, P., Garland, R. M., Wollny, A. G., and Poschl, U.: Relative roles of biogenic emissions and Saharan dust as ice nuclei in the Amazon basin, Nat. Geosci., 2, 401-404, 10.1038/ngeo517, 2009.

Prospero, J. M., Glaccum, R. A., and Nees, R. T.: Atmospheric transport of soil dust from African to South America, Nature, 289, 570-572, 10.1038/289570a0, 1981.

Prospero, J. M.: Long-term measurements of the transport of African mineral dust to the southeastern United States: Implications for regional air quality, Journal of Geophysical Research: Atmospheres, 104, 15917-15927, 10.1029/1999JD900072, 1999.

Prospero, J. M., Collard, F.-X., Molinié, J., and Jeannot, A.: Characterizing the annual cycle of African dust transport to the Caribbean Basin and South America and its impact on the environment and air quality, Glob. Biogeochem. Cycle, 28, 757-773, 10.1002/2013GB004802, 2014.

Prospero, J. M., and Lamb, P. J.: African Droughts and Dust Transport to the Caribbean: Climate Change Implications, Science, 302, 1024, 2003.

Radke, L. F., Lyons, J. H., Hobbs, P. V., Hegg, D. A., Sandberg, D. V., and Ward, D. E.: Airborne Monitoring and Smoke Characterization of Prescribed Fires on Forest Lands in Western Washington and Oregon, USDA Forest Service, Portland, Ore., USA, 81, 1990.

Remer, L. A., Kaufman, Y. J., Holben, B. N., Thompson, A. M., and McNamara, D.: Biomass burning aerosol size distribution and modeled optical properties, Journal of Geophysical Research: Atmospheres, 103, 31879-31891, 10.1029/98JD00271, 1998.

Renard, J. B., Dulac, F., Berthet, G., Lurton, T., Vignelles, D., Jegou, F., Tonnelier, T., Jeannot, M., Coute, B., Akiki, R., Verdier, N., Mallet, M., Gensdarmes, F., Charpentier, P., Mesmin, S., Duverger, V., Dupont, J. C., Elias, T., Crenn, V., Sciare, J., Zieger, P., Salter, M., Roberts, T., Giacomoni, J., Gobbi, M., Hamonou, E., Olafsson, H., Dagsson-Waldhauserova, P., Camy-Peyret, C., Mazel, C., Decamps, T., Piringer, M., Surcin, J., and Daugeron, D.: LOAC: a small aerosol optical counter/sizer for ground-based and balloon measurements of the size distribution and nature of atmospheric particles - Part 1: Principle of measurements and instrument evaluation, Atmos. Meas. Tech., 9, 1721-1742, 10.5194/amt-9-1721-2016, 2016.

Rissler, J., Vestin, A., Swietlicki, E., Fisch, G., Zhou, J., Artaxo, P., and Andreae, M. O.: Size distribution and hygroscopic properties of aerosol particles from dry-season biomass burning in Amazonia, Atmos. Chem. Phys., 6, 471-491, 10.5194/acp-6-471-2006, 2006.

Rizzolo, J. A., Barbosa, C. G. G., Borillo, G. C., Godoi, A. F. L., Souza, R. A. F., Andreoli, R. V., Manzi, A. O., Sá, M. O., Alves, E. G., Pöhlker, C., Angelis, I. H., Ditas, F., Saturno, J., Moran-Zuloaga, D., Rizzo, L. V., Rosário, N. E., Pauliquevis, T., Yamamoto, C. I., Andreae, M. O., Taylor, P. E., and Godoi, R. H. M.: Mineral nutrients in Saharan dust and their potential impact on Amazon rainforest ecology, Atmos. Chem. Phys. Discuss., 2016, 1-43, 10.5194/acp-2016-557, 2016.

Sahyoun, M., Wex, H., Gosewinkel, U., Šantl-Temkiv, T., Nielsen, N. W., Finster, K., Sørensen, J. H., Stratmann, F., and Korsholm, U. S.: On the usage of classical nucleation theory in quantification of the impact of bacterial INP on weather and climate, Atmospheric Environment, 139, 230-240, http://dx.doi.org/10.1016/j.atmosenv.2016.05.034, 2016.

Saturno, J., Holanda, B. A., Pöhlker, C., Ditas, F., Wang, Q., Moran-Zuloaga, D., Brito, J., Carbone, S., Cheng, Y., Chi, X., Ditas, J., Hoffmann, T., Hrabe de Angelis, I., Könemann, T., Lavrič, J. V., Ma, N., Ming, J., Paulsen, H., Pöhlker, M. L., Rizzo, L. V., Schlag, P., Su, H., Walter, D., Wolff, S., Zhang, Y., Artaxo, P., Pöschl, U., and Andreae, M. O.: Black and brown carbon over central Amazonia: Long-term aerosol measurements at the ATTO site, Atmos. Chem. Phys. Discuss., 2017, 1-57, 10.5194/acp-2017-1097, 2017.

Sawyer, A. J., Griggs, M. H., and Wayne, R.: Dimensions, Density, and Settling Velocity of Entomophthoralean Conidia: Implications for Aerial Dissemination of Spores, Journal of Invertebrate Pathology, 63, 43-55, http://dx.doi.org/10.1006/jipa.1994.1008, 1994.

Seinfeld, J. H., and Pandis, S. N.: Atmospheric Chemistry and Physics: From Air Pollution to Climate Change, Wiley, 2006.

Simões Amaral, S., Andrade de Carvalho, J., Martins Costa, M., and Pinheiro, C.: Particulate Matter Emission Factors for Biomass Combustion, Atmosphere, 7, 141, 2016.

Sun, J., and Ariya, P. A.: Atmospheric organic and bio-aerosols as cloud condensation nuclei (CCN): A review, Atmospheric Environment, 40, 795-820, http://dx.doi.org/10.1016/j.atmosenv.2005.05.052, 2006.

Swap, R., Garstang, M., Greco, S., Talbot, R., and Kallberg, P.: Saharan dust in the Amazon Basin, Tellus B, 44, 10.3402/tellusb.v44i2.15434, 1992.

Talbot, R. W., Andreae, M. O., Berresheim, H., Artaxo, P., Garstang, M., Harriss, R. C., Beecher, K. M., and Li, S. M.: Aerosol chemistry during the wet season in central Amazonia- the influence of long-range transport, J. Geophys. Res.-Atmos., 95, 16955-16969, 10.1029/JD095iD10p16955, 1990.

van Hout, R., and Katz, J.: A method for measuring the density of irregularly shaped biological aerosols such as pollen, Journal of Aerosol Science, 35, 1369-1384, 10.1016/j.jaerosci.2004.05.008, 2004.

von der Weiden, S. L., Drewnick, F., and Borrmann, S.: Particle Loss Calculator – a new software tool for the assessment of the performance of aerosol inlet systems, Atmos. Meas. Tech., 2, 479-494, 10.5194/amt-2-479-2009, 2009.

Wang, Q., Saturno, J., Chi, X., Walter, D., Lavric, J. V., Moran-Zuloaga, D., Ditas, F., Pöhlker, C., Brito, J., Carbone, S., Artaxo, P., and Andreae, M. O.: Modeling investigation of light-absorbing aerosols in the Amazon Basin during the wet season, Atmos. Chem. Phys., 16, 14775-14794, 10.5194/acp-16-14775-2016, 2016.

Whitehead, J. D., Darbyshire, E., Brito, J., Barbosa, H. M. J., Crawford, I., Stern, R., Gallagher, M. W., Kaye, P. H., Allan, J. D., Coe, H., Artaxo, P., and McFiggans, G.: Biogenic cloud nuclei in the central Amazon during the transition from wet to dry season, Atmos. Chem. Phys., 16, 9727-9743, 10.5194/acp-16-9727-2016, 2016.

Womack, A. M., Bohannan, B. J. M., and Green, J. L.: Biodiversity and biogeography of the atmosphere, Philosophical Transactions: Biological Sciences, 365, 3645-3653, 2010.

Yamamoto, N., Bibby, K., Qian, J., Hospodsky, D., Rismani-Yazdi, H., Nazaroff, W. W., and Peccia, J.: Particle-size distributions and seasonal diversity of allergenic and pathogenic fungi in outdoor air, ISME J, 6, 1801-1811, http://www.nature.com/ismej/journal/v6/n10/suppinfo/ismej201230s1.html, 2012.

Yañez-Serrano, A. M., Nölscher, A. C., Williams, J., Wolff, S., Alves, E., Martins, G. A., Bourtsoukidis, E., Brito, J., Jardine, K., Artaxo, P., and Kesselmeier, J.: Diel and seasonal changes of Biogenic Volatile Organic Compounds within and above an Amazonian rainforest site, Atmos. Chem. Phys. Discuss., 14, 29159-29208, 10.5194/acpd-14-29159-2014, 2014.

Yu, H. B., Chin, M., Yuan, T. L., Bian, H. S., Remer, L. A., Prospero, J. M., Omar, A., Winker, D., Yang, Y. K., Zhang, Y., Zhang, Z. B., and Zhao, C.: The fertilizing role of African dust in the Amazon rainforest: A first multiyear assessment based

on data from Cloud-Aerosol Lidar and Infrared Pathfinder Satellite Observations, Geophys. Res. Lett., 42, 1984-1991, 10.1002/2015gl063040, 2015.

Zhou, J. C., Swietlicki, E., Hansson, H. C., and Artaxo, P.: Submicrometer aerosol particle size distribution and hygroscopic growth measured in the Amazon rain forest during the wet season, J. Geophys. Res.-Atmos., 107, 10, 10.1029/2000jd000203, 2002.